

# **Fabrication, Testing and Analysis for Non-destructive Inspection of Bonded Composite Joints**

A Dissertation  
Presented to  
the Academic Faculty

by

Michael McCracken

In Partial Fulfillment  
Of the Requirements for the Degree  
Master of Science in Mechanical Engineering in the  
George W. Woodruff School of Mechanical Engineering

Georgia Institute of Technology

December of 2019

**COPYRIGHT © 2019 BY MICHAEL MCCRACKEN**

# **Fabrication, Testing and Analysis for Non-destructive Inspection of Bonded Composite Joints**

Approved by:

Dr. Massimo Ruzzene, Co-Advisor  
School of Mechanical Engineering  
*Georgia Institute of Technology*

Dr. Chuck Zhang, Co-Advisor  
School of Industrial and Systems Engineering  
*Georgia Tech Institute of Technology*

Dr. Yan Wang  
School of Mechanical Engineering  
*Georgia Institute of Technology*

Date Approved: December 5, 2019

## ACKNOWLEDGEMENTS

I would like to acknowledge first the sponsors who helped make this work possible, Lockheed Martin with Dr. Steve Engelstad's oversight and Delta Air Lines with Mr. Nathan Schulz. I am thankful that through the funding, I could work on a meaningful, interesting project that I enjoyed have the opportunity to work on.

I am thankful to my co-advisor Dr. Massimo Ruzzene for being willing to be my co-advisor and being flexible and available to me to help me get this thesis completed.

Dr. Chuck Zhang, thank you for being my co-advisor as a master's student. I appreciate the pushes that you gave me to work harder and the environment of fellowship you built for your students. This research and paper could not have been completed without your guidance.

Thank you to Dr. Yan Wang for being on my reading committee and your valuable comments on this thesis.

I would also like to thank Jarod Weber for always being helpful, available, and caring with all the work we did. In addition, I would like to thank several students that I worked with including Adam Baker, Jialei Chen, Zeke Liu, Sean Mou, Jenny Tian.

I'd like to thank my family for encouraging me my whole life in my passion of all things math, physics, and engineering.

I would not be able to do write this without all of the support of my beautiful wife Mallory. I am so grateful for the blessing you are to me and all you have done for me.

Finally, I'd like to thank the Lord for giving me the ability to do this work, a joy for discovery, and a peace that surpasses all understanding. Soli Deo gloria.

# Table of Contents

<b>ACKNOWLEDGEMENTS .....</b>	<b>iii</b>
<b>Lift of Tables .....</b>	<b>v</b>
<b>List of Figures.....</b>	<b>vi</b>
<b>SUMMARY .....</b>	<b>1</b>
<b>INTRODUCTION.....</b>	<b>2</b>
Background.....	2
Related Work in Detection of Composite Bond Defects .....	5
<b>METHODS .....</b>	<b>20</b>
Test Coupons Specifications and Fabrications Process .....	20
Mechanical Testing of Test Coupons .....	27
<b>RESULTS AND DISCUSSION .....</b>	<b>42</b>
<b>CONCLUSIONS .....</b>	<b>60</b>
<b>References .....</b>	<b>63</b>

## Lift of Tables

Table 1: Water contact angle trends.....	15
Table 2: Material 1 lap joint normalized data sample 1-20 .....	47
Table 3: Material 1 lap joint normalized DCB data samples 21-40 .....	48
Table 4: Material 1 lap joint normalized data sample 41-60 .....	49
Table 5: Material 1 normalized DCB data sample.....	53
Table 6: Material 2 normalized DCB data samples 1-20.....	56
Table 7: Material 2 normalized DCB data sample 21-37 .....	57

## List of Figures

Figure 1: Composites in commercial airframes [4] .....	3
Figure 2: Scarf repair [24].....	10
Figure 3: 3D DIC setup.....	13
Figure 4: Painted speckle pattern on test sample .....	13
Figure 5: Reference and deformed subset illustration [39].....	14
Figure 6: Contact angle examples.....	15
Figure 7: Several molecular vibrational modes [51].....	17
Figure 8: Radiation exciting carbonyl bond to its excited state [51] .....	18
Figure 9: Raw FTIR output data .....	18
Figure 10: CFRP layup .....	21
Figure 11: DCB sample .....	22
Figure 12: Lap joint sample .....	23
Figure 13: Test frame and 3D DIC setup.....	28
Figure 14: DCB sample being tested .....	29
Figure 15: Material 1 normalized raw lap test data .....	30
Figure 16: Material 1 normalized raw DCB test data .....	30
Figure 17: Material 2 normalized raw DCB test data.....	31
Figure 18: DIC image showing point and field strain measurement .....	32
Figure 19: DIC image showing the surface mesh.....	32
Figure 20: DIC image showing accurate distance measurement between two points.....	33
Figure 21: Surface Analyst contact angle images for higher contact angle.....	36

Figure 22: FTIR examination of sanding and isopropyl alcohol on Material 1.....	37
Figure 23: Unsanded Material 1 2D view of surface .....	38
Figure 24: Unsanded Material 1 3D view of surface .....	39
Figure 25: Sanded Material 1 2D view of surface .....	40
Figure 26: Sanded Material 1 3D view of surface .....	41
Figure 27: Three failure modes, (a) adhesive, (b) adherend, and (c) cohesive.....	43
Figure 28: Failure modes on actual DCB sample .....	44
Figure 29: Material 1 lap joint failure stress plotted against contact angle .....	45
Figure 30: Normalized average failure stress for pristine, all, and heavily contaminated Material 1 lap joint samples .....	46
Figure 31: Material 1 normalized DCB fracture toughness plotted against contact angle	51
Figure 32: Material 1 normalized pristine and contaminated DCB average fracture toughness.....	52
Figure 33: Material 2 DCB normalized fracture toughness plotted against contact angle	54
Figure 34: Material 2 normalized pristine and contaminated DCB average fracture toughness.....	55
Figure 35: Failure modes for (a) contaminated and (b) pristine DCB samples .....	59

## SUMMARY

Carbon fiber reinforced polymer (CFRP) has risen in usage among many industries including aerospace, automotive, and wind energy. CFRP is used structurally due to its light weight, corrosion resistance, and mechanical properties. However, there are large differences between CFRP and conventionally used metals. One major issue with using CFRP is creating a reliable bonded joint for joining and repair applications during both manufacturing and services/maintenance. For various reasons, using conventional fasteners is not desirable for creating CFRP joints. Instead, adhesives are widely used to bond CFRP to other materials. Adhesive bonding is not nearly as well understood as conventional fastening. Because adhesives are not well understood, it is difficult to determine how reliable an adhesively bonded joint is. One effective way of assessing the bond reliability is through non-destructive inspection (NDI). There are currently no effective NDI methods available for detecting a “kissing bond,” a bond that has physical contact with the adherend, but very little interfacial strength. Kissing bonds form unexpectedly and can cause a disbond under loads much smaller than expected. In order to study kissing bonds and their detection, these weakened bonds must be reliably fabricated in a controlled environment. In order for NDI detection of kissing bonds to be studied effectively, it must be tested on bonded joints which have been fabricated in a controlled manner. This thesis presents a method of controlled fabrication which can produce reliably strong and weak kissing bonds, specifically for the purpose of NDI research in mind.

# INTRODUCTION

## Background

The use of CFRP has greatly increased over the last several decades, particularly in the aerospace and automotive industries. Two recent airplanes, the Boeing 787 and Airbus A350, are recent examples of this. The 787 is 50% composite by weight, and the A350 is 53% composite by weight [1][2]. The trend of increasing use of composites in airplanes can be seen clearly in Figure 1. In the automotive industry, there are the BMW i3 electric vehicle and the i8 high performance sports vehicle. Both these vehicles have a significant proportion of the structure made with composite materials. The i8 in particular has a chassis that is fully carbon composite. The front and rear crash structures are still metal, though [3]. However, even with this trend of growing use of composites, the materials are not nearly understood as well as conventional materials, like metals. Some advantages of CFRP is its corrosion and fatigue properties, but impact can be a much larger issue in CFRPs than in metals. CFRPs have less favorable qualities for resisting impact. Metals tend to be quite ductile, and they can absorb more energy from an impact than CFRPS. CFRPs are more brittle and therefore impact causes more damage to the material [3]. Not only are they more brittle, but after an impact non-surface layers of the composite may be damaged while surface layers “bounce back” causing there to be no visible damage on the surface. Causes of damage to a commercial transport aircraft could arise from a dropped tool by a mechanic, a collision with a truck while grounded, objects thrown up on the runway, lightning strikes, bird strikes, environmental debris like hail,

fatigue, moisture, thermal loading, etc. [3]. The auto industry also can have issues with impact due to other vehicles, debris kicked up from the road, environmental debris, or collisions with other objects. Similarly, in the wind energy industry, bird strikes, and environmental debris can damage the turbine blades. CFRPs are increasingly used not only in the aerospace industry, but also being used more in the in the automotive industry, for wind energy, and for pressure vessels and pipes, among other uses.

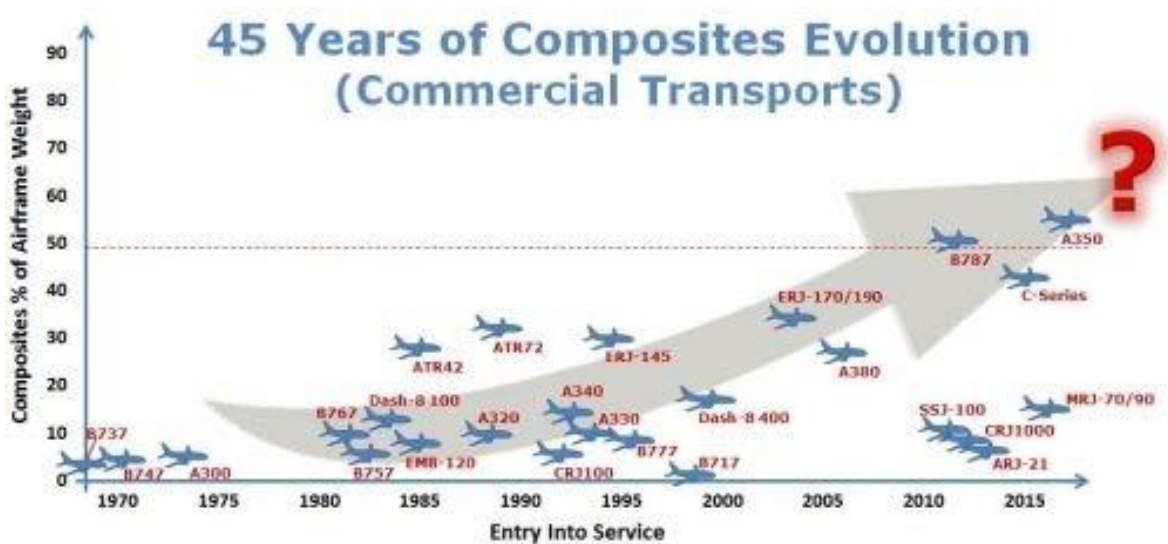


Figure 1: Composites in commercial airframes [4]

CFRPs are typically bonded with adhesives instead of fastened conventionally.

One reason for the use of adhesives is for the mechanical advantage. Instead of fastening

distinct points, a large region can be bonded together. Where conventional fasteners will have stress concentrations at the fasteners, the adhesive will have the stress distributed throughout the area of the bond [5]. Reducing stress concentrations is almost always favorable in structures. Another advantage is that it is not necessary to drill or cut into the CFRP. Drilling into the CFRP can at best weaken the structure and at worst damage it beyond use. Drilling can cause delamination or micro-damage which can be the nucleation point for larger damages [6][7][8]. Currently, however, fasteners are still widely used in industry for bonding flight critical components along with adhesives in order to create joints. The reason for this redundancy in joining is regulation by the FAA due to a lack of knowledge on the reliability of adhesive bonding. The FAA currently enforces airplanes needing additional design features on flight critical bonded areas, which would be fasteners. The FAA also state that they could allow validation of the bond strength through the use of NDI instead of using fasteners as a fail-safe. However, the FAA admits that this rule is intended to be left open for future advancement, because currently there is no such technology matured enough [9]. Because of this regulation on aviation, manufacturers and commercial transport companies must spend time and materials to add extra fasteners to already bonded composites. The extra fasteners add weight to the aircraft which will can cause more difficulties in the design and more cost to operate due to increased fuel cost for the extra weight. Those are not the only drawbacks, but also by drilling fasteners through the CFRP, the composite is also weakened. So, the extra fail-safes added by the FAA cost companies not only time and money, but it also makes their CFRP parts weaker than if they did not have the fail-safes.

An NDI method that could detect “kissing” bonds would, therefore, be immensely desirable for industry.

A kissing bond is one of the major problems or defects in adhesive bonding today. A kissing bond is defined as a bond where there is “intimate” contact between the adhesive and adherend surfaces, yet with very little interfacial strength [10]. Another functional definition of the kissing bond is broken into three criteria. First, the bond strength must be less than 20% of full strength. Second, the failure mode must be 100% adhesive. Third, a normal incidence L-wave ultrasonic signal must not exhibit low-signal attenuation [11]. This means that ultrasonic testing would not be able to detect any weakness or would act as if there is no disbond. The literature suggests that the causes of kissing bonds may be lack of full curing of the adhesive, surface contamination, or physical damage [12].

### **Related Work in Detection of Composite Bond Defects**

Kissing bonds are difficult to detect using current NDI methods. Kissing bonds are such a major issue and are so difficult to measure using NDI, that finding an NDI method for identifying kissing bonds has been described as the “Holy Grail of inspection” [13]. The purpose of NDI is to locate damage in composite structures and assess the size and type of damage. There are many different methods for NDI. A list of these technologies includes visual inspection, tap testing, ultrasonic testing, laser-ultrasonic testing, thermography, digital shearography, x-ray radiography, terahertz 3D

imaging, acoustic emission, and laser bond inspection (LBI). None of these NDI methods can find all types of damages, and currently none of them can detect kissing bonds. For example, conventional ultrasonic inspection is able to detect voids and disbonds but cannot detect kissing bonds because there is no void due to the intimate contact. Ultrasonic methods have been studied since the 1960s due to their ability to obtain information on the morphological and elastic features at the interface of adhesive bonds by how the ultrasonic waves propagate [14]. The mechanical behaviors of the materials, such as the modulus, nonlinear stress-strain behavior, etc. are linked to the behavior of the ultrasonic wave [15].

Harmonic imaging, or nonlinear harmonics, functions by generating a nonlinear wave with an amplitude large enough to cause local deformation in the adhesive bond. This is due to the binding force of the adhesive is nonlinear. The technique is still immature, especially for epoxy based composite materials with weak bonds, according to leading researchers in the field [16]. Theoretically, the mechanical behavior of the adhesive can become linear during failure. This transition from nonlinear to linear mechanical behavior can be considered a dividing line between strong and weak bonds [17]. However, harmonic imaging has a large measurement error from all sources, such as the measuring device, probes, bonded materials, etc. This noise created can be larger than harmonic signals required to detect strong or weak bonds, and the harmonic signal can be difficult to isolate.

Guided wave ultrasonic technique is performed using two transducers for the the emission and reception of the waves. It is a variant of oblique incidence techniques. By having the wave reflected several times inside the material before reaching the reception

transducer, much is revealed about the properties of the sample. One group of researchers suggest that if two materials have a large difference in acoustic impedance, then weak bonds can be detected [18]. This could therefore not apply to an epoxy based composite bonded with an epoxy adhesive.

Shear wave resonance is a technique specifically for adhesive bonds in metallic materials. The theory is based on the assumption of longitudinal sound velocity being twice the shear sound velocity in a metallic material. If this is true, then the thickness-shear resonances with motions relatively parallel to the surface occur. This can be used to observe the adhesive bond. This has been used to detect kissing bonds in bonded aluminum samples [11], however no study with this technique for composite material has been found.

Thermography is the use of examining the temperature of a bond under load in order to learn about that bond's strength. The fracture activation energies are different for weak and normal adhesive bonds theoretically [19]. The difference in activation energy corresponds to the heat generated under stress and the degree of polymer bonding. This relationship is the motivator for thermography methods.

Shearography is when light or sound waves are used to gather information about the surface of a sample. The light field is scattered from an object onto a recording medium. The object will then be subjected to some load. The deformation on the surface with the light still scattered across it can be used to create a reconstructed and interfered light field. The fringes of the reconstructed field can be used to infer the displacement field on the surface of the object. A similar method, holographic interferometry, has been

used to inspect adhesive bonds with and without discontinuities [20]. This method shows some promise, but a setup for practical use has not been developed.

LBI uses a high powered laser to generate shock wave with short pulses on the surface of the area. The shock wave generates compressive and then tensile forces throughout the area [21-23]. LBI is a new and promising technology. The notion is that the weak bonds will be disbanded by the shock wave without damaging strong bonds. LBI has been found to detect many types of defects in composite materials [11,15]. Overall, LBI is a newer technology that is still being evaluated for practical industrial purposes and is not ready for large scale rapid testing. As more research is required using NDI on weak bonds in order to detect kissing bonds, it is necessary to create controlled weak bonds.

Adhesive bonds are typically used in repair of composite parts when the damage is small. Part of the reason for this is regulation by the FAA on flight critical parts requiring extra design features for safety. In order to adhere the adhesive, the adhesive is typically cured. The curing process involves heating the desired bonding area and subjecting it to increased pressure. When the adhesive is being used to bond an area, the curing may be done in an autoclave or outside of an autoclave. An autoclave is a container that creates high temperatures and pressures inside of itself. Autoclaves large enough to place plane parts in them can be extremely expensive to purchase and operate. The bond will depend on the composite material and adhesive used. Typically, out-of-autoclave composites are used for repairs because they do not require the use of a large autoclave. Out-of-autoclave bonding is typically performed with a single heat source, like

a heating pad, with a sealed bag around the repair area in order to achieve vacuum pressure.

A typical repair that may be performed on the skin of an airplane in industry is scarf repair. One of the reasons scarf repair is preferable is that it has a very small, if any, effect on the aerodynamic properties of the repair area, and also does not cause a larger stress due to discontinuities. Scarf repair is performed by removing the original material until the damage is fully removed, while also removing composite from the area in a stepped or tapered manner around the damaged area. Then the number of plies and their boundaries are identified. The repair patch will contain the same number of plies in a similar size in order to create a patch as shown in Figure 2. Next the adhesive, and possibly the CFRP patch also, is cured, and the area is sanded and finished [3]. The value  $D$  in Figure 2 is dependent on the size of the damage, while the angle of the scarf repair,  $\theta$ , and  $L$  is dependent on the strength of the bond. Because it is difficult to create bonds of reliable strength a larger safety factor is necessary for the scarf bond. This means that more of the original material is removed, causing more time to do so, and that more new material is required to replace it, which causes the repair to have a higher cost. A bond with a more reliable strength could therefore have a smaller more appropriate safety factor.

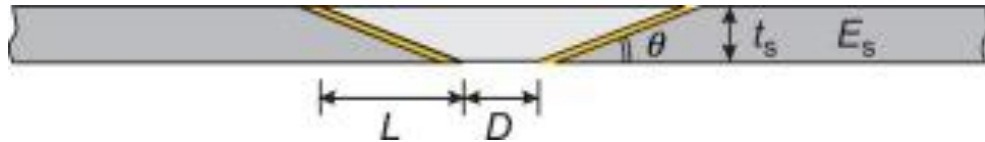


Figure 2: Scarf repair [24]

One of the most crucial factors in creating a reliable bond is the surface preparation. Factors of surface preparation include controlling environmental factors such as the ambient temperature, humidity, and the particles in the air. Another factor is the cleanliness of the adherend surface itself. However, because of the chemical aspect of the adhesive bonding, the chemicals used for cleaning are therefore also important. Some common methods of surface preparation are using a peel ply layer, solvent, abrasive techniques such as sanding, atmospheric plasma and laser treatments [3]. For abrasive techniques in particular, the quality of the preparation is highly dependent on the operator and can be very labor intensive. However, abrasive techniques can remove contaminants from the surface. Even still, abrasive techniques are still widely used [25]. Therefore, optimizing the amount of surface preparation will allow for less wasted operator time.

One of the similar efforts seen in industry and government research is the Transition Reliable Unitized Structure (TRUST) project lead by Lockheed Martin with the sponsorship of DARPA [26]. The goal of the TRUST project is similar in attempting to create more trust in the adhesive bond strength. TRUST is using large data sets and Bayesian process control. The TRUST report is not intended to remove all uncertainty, but to quantify it. TRUST also tested on DCB samples based off of ASTM D5528, like

the research presented in this paper. The TRUST report tested on a large data set of 600 DCB samples [26]. However, TRUST did not use the type of contaminant that is used in the research presented in this paper.

There is not much research found in controlled fabrication of adhesive bonds. There is research looking at the effects of certain factors on bond strength such as the adhesive and substrate dimensions [27] or use of certain plasma treatment methods [28]. However, there is not a comprehensive coupon fabrication method put forward previously. There is research that looks at another Frekote mold release agent as a contaminant [29]. This work looks at contaminating only a sample of the bond area and is not focused on a comprehensive fabrication and contamination method.

Digital image correlation (DIC) is a method for measuring the deformation of a surface. Where a mechanical test frame will typically only record the displacement and force during a test, if the test were coupled with a DIC system, then the surface deformation, strain, and stress can all be found across the surface of the sample. DIC can be favorable to other strain or displacement measuring methods because of its ability to measure across the entire surface of the sample. This could be favorable compared to strain gauges or an extensometer which can only measure values at certain points. DIC was first developed in the 1980s by researchers at the University of South Carolina [30]. Sometimes DIC can be referred to as other names, such as electronic speckle photography [31,32], texture correlation [33], digital speckle correlation method [34,35], and computer-aided speckle interferometry [36,37]. DIC can be used on both 2D and 3D surfaces [38]. DIC is also a non-contact measurement method, depending on the surface of the sample. If the surface of the sample has a surface with a random gray intensity

distribution, then no sample preparation is necessary. However, if this is not true then paints can be applied to the surface of the sample [39]. Because DIC uses digital images to process the data, there is an extremely wide range resolutions, sample sizes, and test speeds. The constraining factor is whatever captures the images. For example, DIC has been used with scanning electron microscopes [40-42] and with high speed recording equipment [7,43]. A 3D DIC setup can be seen in Figure 3. DIC requires some distinct pattern on the surface of the sample in order to track. An example image can be seen in Figure 4. The DIC method involves first taking a distinct subset of the image, as seen in Figure 5. The subset is then tracked in the deformed image and compared to the original image. The displacement and strain can then be easily calculated once the subset has been determined in the deformed image. One of the weaknesses of DIC is identifying the subsets at discontinuities. For this reason, in fracture mechanics the data ahead of the propagating crack is used, as data at the discontinuities is often unreliable.



Figure 3: 3D DIC setup



Figure 4: Painted speckle pattern on test sample

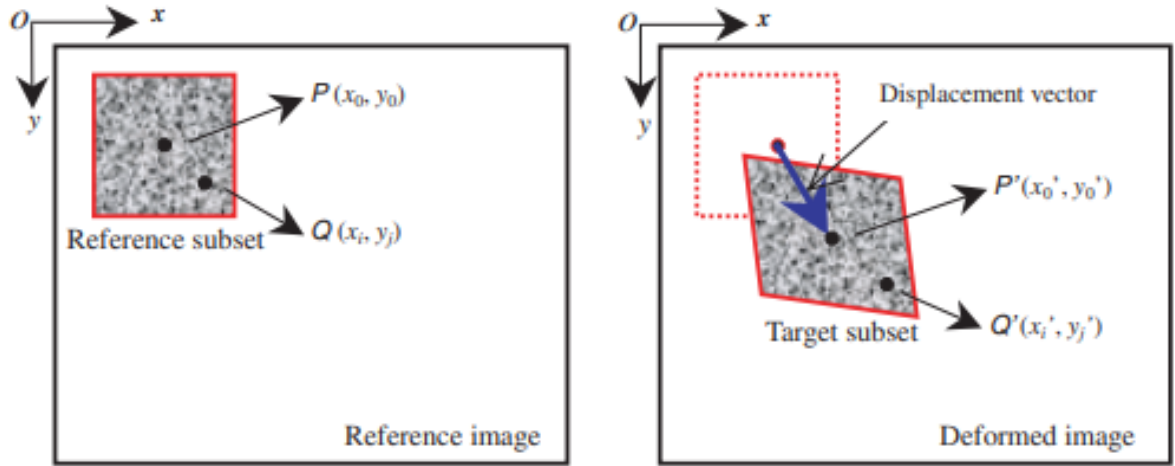


Figure 5: Reference and deformed subset illustration [39]

A method for determining how well an adhesive will adhere to the substrate is using water contact angle measurements. This method measures the angle that the surface of water will make with the surface of the sample, as seen in Figure 6. The contact angle of the water is related to the surface energy of the solid according to the equation:

$$\gamma_{LV}\cos\theta = \gamma_{SV} + \gamma_{SL}$$

where  $\gamma_{LV}$  is the surface tension for the liquid-vapor,  $\theta$  is the contact angle,  $\gamma_{SV}$  is the free surface energy, and  $\gamma_{SL}$  is the solid-liquid surface tension [44]. There is much documentation for common materials'  $\gamma_{LV}$  values. Research involving relationships between contact angle and adhesion strength has been going on for decades [45]. Table 1 shows the relationship between contact angle and select properties.



Figure 6: Contact angle examples

Table 1: Water contact angle trends

Smaller	Contact angle	Larger
Better	Wettability	Worse
Better	Adhesiveness	Worse
Larger	Solid surface free energy	Smaller

One tool that is beneficial in the examination of adhesive bonding is the Fourier-transform infrared (FTIR) spectroscopy. The FTIR can characterize the chemical composition of the surface of a sample. The FTIR technique uses IR radiation and can record the surfaces interaction with the radiation [46]. FTIR is a useful technique for surface characterization because it non-destructive, gives real-time measurement and is

not complicated to operate. Infrared spectroscopy has three primary regions. The near-infrared (NIR), which is associated with the wavenumber range of  $14000 - 4000 \text{ cm}^{-1}$ , can excite overtone or harmonic vibrations. The mid-infrared (MIR), which is associated with wavenumber range of  $4000 - 400 \text{ cm}^{-1}$ , is used to study fundamental vibrations and associated rotational-vibrational structure [47]. The far-infrared (FIR), which is associated with the wavenumber range of  $400 - 10 \text{ cm}^{-1}$ , has low energy due to being near the microwave radiation region and is used for rotational spectroscopy. The fundamental frequency absorption band of most chemicals are found in the MIR region, which is used in this research.

In order to explain how FTIR works, a covalent bond will be used as an example. Molecules are always in motion, with many different modes of vibrations, such as symmetric and asymmetric stretching, bending, twisting and rocking. Some of these modes can be seen in Figure 7. The FTIR will radiate infrared radiation of a certain range of wavenumbers. The chemical bonds will only absorb the radiation around its characteristic frequency which corresponds to the specific chemical bonds, as seen in Figure 8. In this case, the amplitude of the vibration increased. The difference in energy in the ground state and excited state is associated with the wavenumber of the energy that was absorbed. This is the basis of how the FTIR measures information about the bonds. It sends out infrared radiation at specific frequencies, and then measures the amount of radiation that is reflected back from the sample. The theory is that frequencies that are not returned must have been absorbed by the sample. Therefore the frequencies that are not returned must correspond to specific chemical bonds from the surface of the sample [48-

50]. Conventionally the raw data from the FTIR will be the absorbance plotted against the wavenumber. An example of FTIR data can be seen in Figure 9.

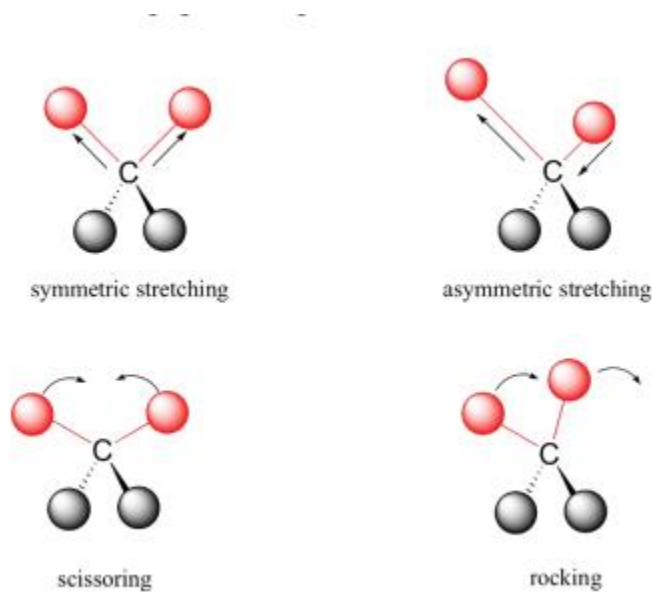


Figure 7: Several molecular vibrational modes [51]

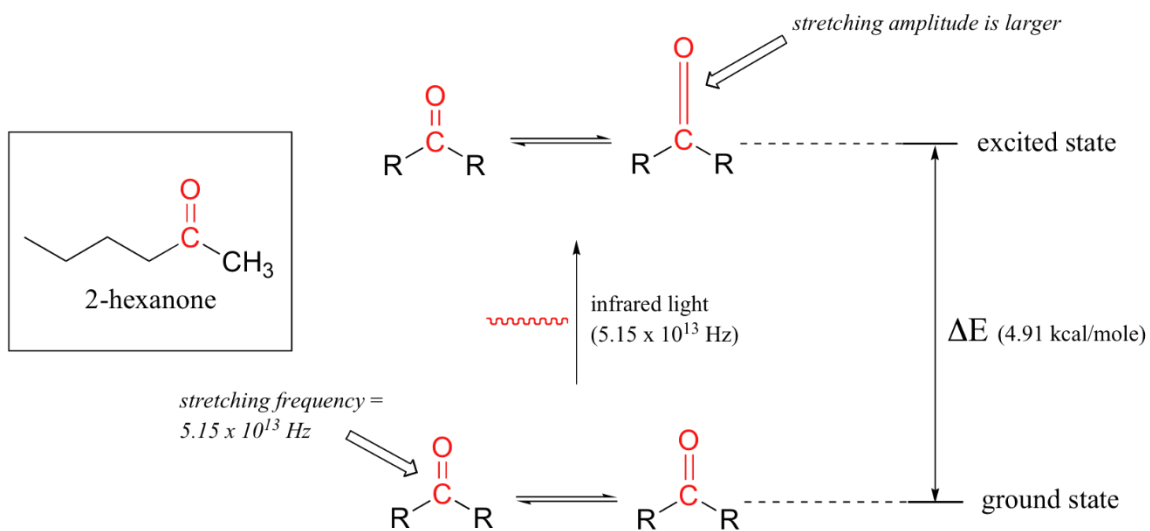


Figure 8: Radiation exciting carbonyl bond to its excited state [51]

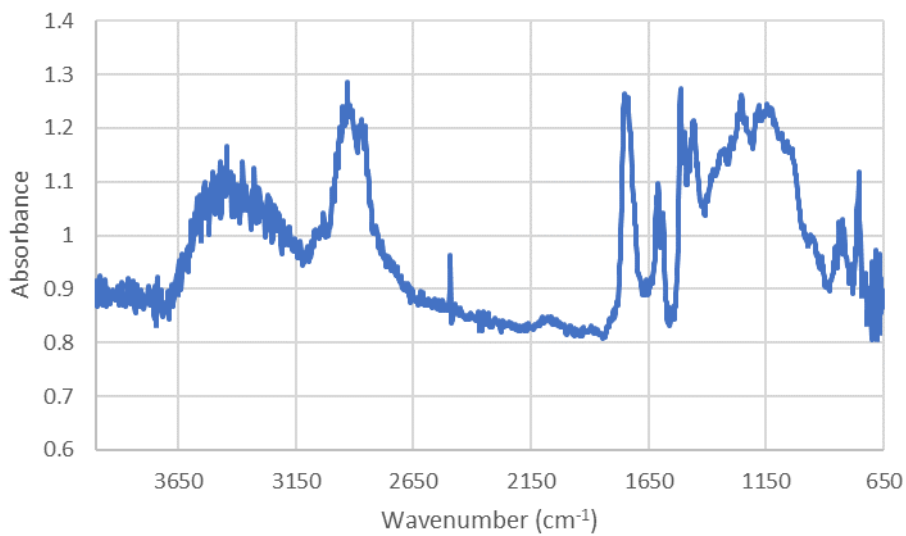


Figure 9: Raw FTIR output data

The purpose of this research specifically is to create a controlled method of fabrication for composite adhesively bonded joints with the purpose of being used NDI research. For example, there is ongoing collaborative research between a research group in the Georgia Tech Aerospace School about NDI, with Dr. Massimo Ruzzene. That research project investigates the use of lamb waves for NDI of composite adhesively bonded joints. The controlled composite joint fabrication data and mechanical testing data is correlated with the results of the NDI tests in order to evaluate the NDI method.

There is a need for a reliable method to fabricate adhesively bonded CFRP joints for testing, especially for NDI application. This fabrication method will add reliability in the fabrication of CFRP coupons for testing. This will facilitate NDI research in its study of the kissing bond. Using water contact angle measurements as the primary criterion and check throughout the fabrication process allows for reliable and quick evaluation of the bond throughout the fabrication process for strong and very weak bonds. The method will describe that fabrication method for reliable kissing bonds and pristine bonds.

## **METHODS**

The goal of the fabrication and testing process was to create a controlled process to produce bonded coupons with reliably created strong and weak bonds. Therefore, through literature and discussions with industry professionals, the following method was developed. The completed lap joint and DCB test sample, fabricated according to its appropriate ASTM standards [52] [53] can be seen in Figure 11 and Figure 12, respectively. The lap shear test was chosen due to its prevalence in adhesive bonding tests, as seen by Davis and Tomblin who found that in 20 organization, 77 percent of designers use lap shear test results in order to establish what is acceptable for design [54]. The DCB test was used also due to its capability to determine the failure mode and fracture toughness.

### **Test Coupons Specifications and Fabrications Process**

The process began with the fabrication of the coupons beginning with the uncured prepreg material. Two materials were used, an out-of-autoclave material and an autoclave material. The out-of-autoclave material will be referred to as Material 1, and the autoclave material will be referred to as Material 2. The prepreg was first cut from the roll using scissors and a metal 12"x12" square as a template. The material was cut out in such a way that the fibers are oriented in a 0/90 degree orientation or a  $\pm 45$  degree orientation. The layers of the cut out prepreg were then placed together in a layup using 6

0/90 degree oriented plies and 5  $\pm 45$  degree oriented plies for a total of 11 plies, as shown in Figure 10. The number of plies was chosen based on conversations with industry professionals. The layup was then created by alternating between the ply orientations beginning with the 0/90 degree ply, such that the layup code will be as follows:  $[(0/90, \pm 45)_2, \overline{0/90}]_s$ . This layup allows for simplicity due to the layup being symmetric and balanced. Because of the angles used and the layup, the material can be said to have quasi-isotropic properties in-plane.

0/90
$\pm 45$
0/90

Figure 10: CFRP layup

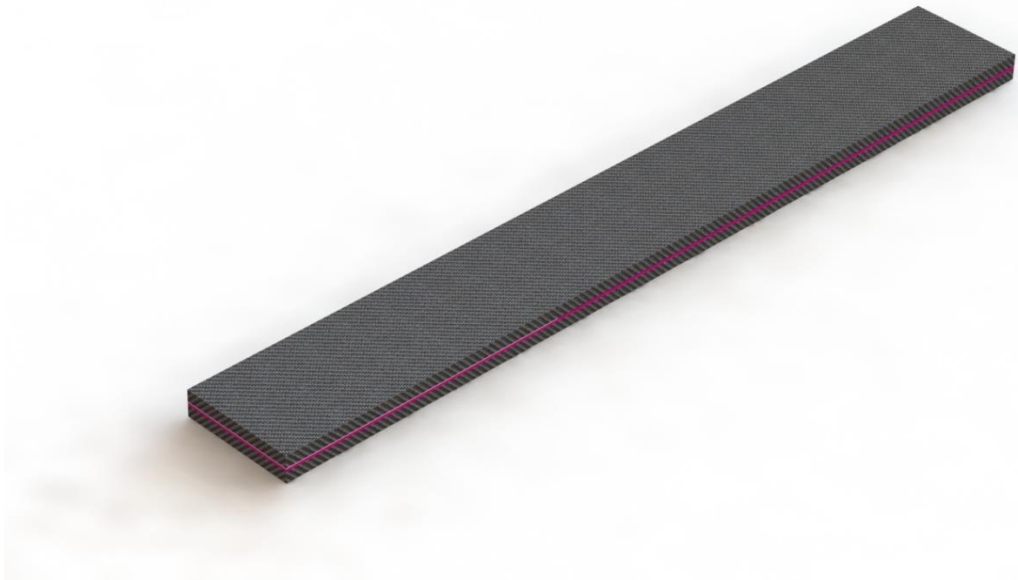


Figure 11: DCB sample

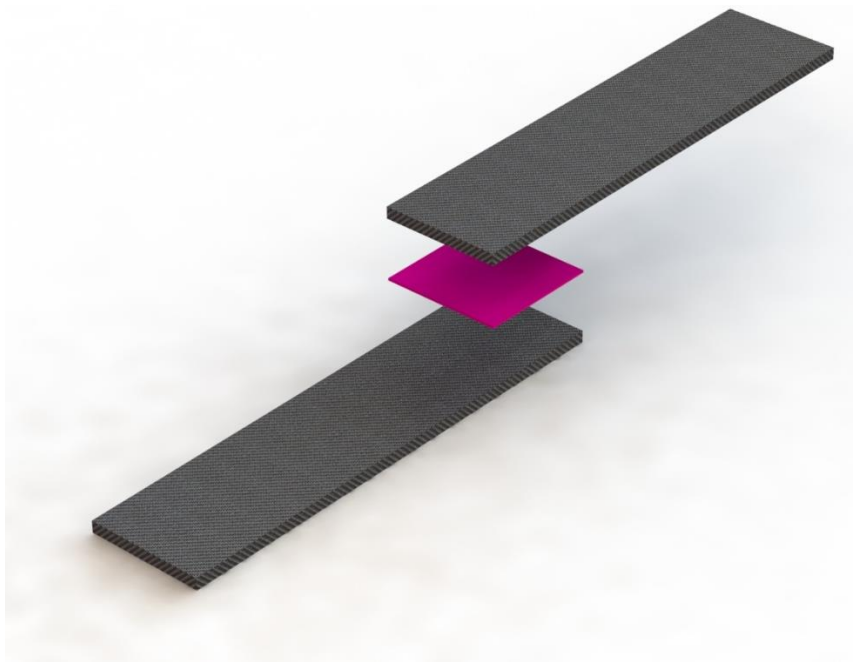


Figure 12: Lap joint sample

Next the out-of-autoclave layup is cured using a HEATCON HCS9000B Single Zone Hot Bonder, referred to as the hot bonder. One of the reasons this unit was chosen

was due to its wide application in industry. The hot bonder has a blanket that can heat itself to specified temperatures that have been programmed according to the prepreg material specifications set by the manufacturer. The hot bonder will also pull vacuum pressure. The heat blanket and laminate are sealed with a vacuum bag and then a minimum vacuum pressure of 22 inHg is applied. The temperature cure cycle, vacuum pressure, ambient temperature, humidity, and prepreg out-time were recorded during this step. The out-time is the cumulative time spent outside of the freezer before bonding. All materials stored in a freezer must be sealed while in the freezer and brought to room temperature before being unsealed.

After the curing of the panel, the samples are then cut according to the test specifications. The panels are cut using a DREMEL 4300 rotary tool by hand into the desired test coupon size. This method was found to not cause delamination during the cutting process or any unwanted damage. Other cutting methods, such as a waterjet, were tested briefly, but were found to cause delamination. It may be possible to use a waterjet for cutting the composite, but the rotary tool was used for expediency. This is a step that would likely not be used in the aerospace industry because the uncured prepreg would already be cut into the desired size and geometry.

Once the coupons were created, the surface preparation and characterization process began. The samples were sanded using 220 grit sandpaper by hand or 120 grit if sanded using an orbital sander. For consistency, one ply was sanded off of the bonding side of the CFRP. This method was used to remove any surface contaminants. Due to the changing orientation of the ply, it is visibly apparent when one ply is removed, and the next ply below is showing. The surface is then wiped using SCRUBS citrus degreaser

towel. This towel was found to create low contact angles and discussing with industry professionals. The sample was wiped in the same direction so as to not re-contaminate with carbon fiber dust. The samples were wiped until no sanding residue was seen on the solvent wipe. The samples were then left to air dry until the solvent had completely evaporated.

Once evaporated, the contact angle measurements were taken. For the lap joint samples, one contact angle measurement was taken in the bonding area of each coupon. For the DCB samples, three contact angle measurements were taken across the test area of each coupon. Then the contamination was added to certain samples. The mold release agent contaminant was applied across the surface of the contaminated coupon. For most samples, the contaminant was applied to one coupon in order to create one interface that was weaker than the other. The mold release agent contaminant chosen was Loctite Frekote 44NC because of information found in a presentation by researchers at Florida International University [55]. The mold release agent also contains siloxane functional group, which can create weak bonds [56]. Mold release agents are also products that could be found in an industrial CFRP fabrication area, which means contamination from the mold release agent could happen in an industrial setting. The coupon is left to then air dry. Contact angle measurements are taken in a similar manner as before, with one on the lap joint sample, and three across the DCB sample. For the DCB sample, it was decided that the contact angle must be within  $\pm 3^\circ$  from each other point measured on that sample. If necessary, the samples were contaminated more, or they were cleaned and then re-contaminated.

Once dry, the samples were assembled according to the appropriate standard[52][53]. The DCB sample is assembled with the two 7.5"x1" CFRP coupons and a 7.5"x1" adhesive strip. A 2.5"x1"x0.0005" non-adhesive insert is placed at one edge where the load will be applied, as seen in Figure 11. The lap joint sample is assembled using two 4"x1" CFRP coupons, and a 1"x1" adhesive strip as can be seen in Figure 12. Both samples used the same type of adhesive. The adhesive out-time is recorded. The samples are then cured using the hot bonder. The setup process is similar to curing the prepreg. The adhesive is cured according to the manufacturer's specifications. Once the adhesive is cured, the samples are ready for mechanical testing, except for additional steps in order to use the DIC. In order for the DIC to work, a speckle pattern needs to be created on the surface. The pattern is created using a black and a white spray paint. The black spray paint is Quick Color Spray Enamel, and the white spray paint is Rust-oleum Enamel. The spray paints were chosen because it was an enamel paint. Enamels are not glossy and therefore do not create as much of a glare. This is desirable during the DIC testing because a glare on the surface results in no DIC data gathered from that area. Several spray paints were tested in order to find a brand and painting method which would work well with the DIC. The finer the speckle pattern, the higher the resolution data the DIC can get, as long as the DIC can still distinguish between distinct features. In order to create a fine speckle pattern, an initial layer of white paint is sprayed on the surface to cover the entire surface of the measured region, shown in Figure 4. Then the black spray paint is sprayed from roughly a foot away from the sample in order to not create a mist of black paint. The choice of white spray paint was not as important, because all that was needed was an enamel paint to completely cover

the surface of the sample. The black spray paint was chosen due to how the paint was sprayed out of the can in order that it can create a mist so as to create a good speckle pattern. A sufficient speckle pattern was determined visually. If necessary, the painting process is repeated. However, repeating the painting process is not desirable because the DIC measures the deformation of the paint. The more layers of paint on the surface of the sample, the more the CFRP surface deformation is distorted by the deformation in the larger amount of paint.

### **Mechanical Testing of Test Coupons**

The mechanical testing was done using a Shimadzu AG-20kN/50kN ICD. During the mechanical testing, the DIC was used in order to record surface strain throughout the test. The load cell recorded the time, force, and displacement. The test setup is shown in Figure 13. The lap joint samples were placed in clamps that put a tensile load on the samples until failure. The failure was always a sudden failure for the lap joint samples. The DCB samples were adhered to loading blocks at the end with the non-stick slip. To adhere the DCB sample to the load blocks, Gorilla super glue gel, was used. The DCB test can be seen in Figure 14. The normalized raw load cell lap data can be seen in Figure 15. The normalized raw load cell Material 1 DCB data can be seen in Figure 16. The normalized raw load cell material 2 DCB data can be seen in Figure 17. An example of what the DIC postprocessed images of the surface strain and point strain measurement can be seen in Figure 18 and Figure 19. During the data reduction, the DIC distance

measurement tool is extremely valuable due to its ability to measure distances to the nearest thousandth of a millimeter, as can be seen in Figure 20.

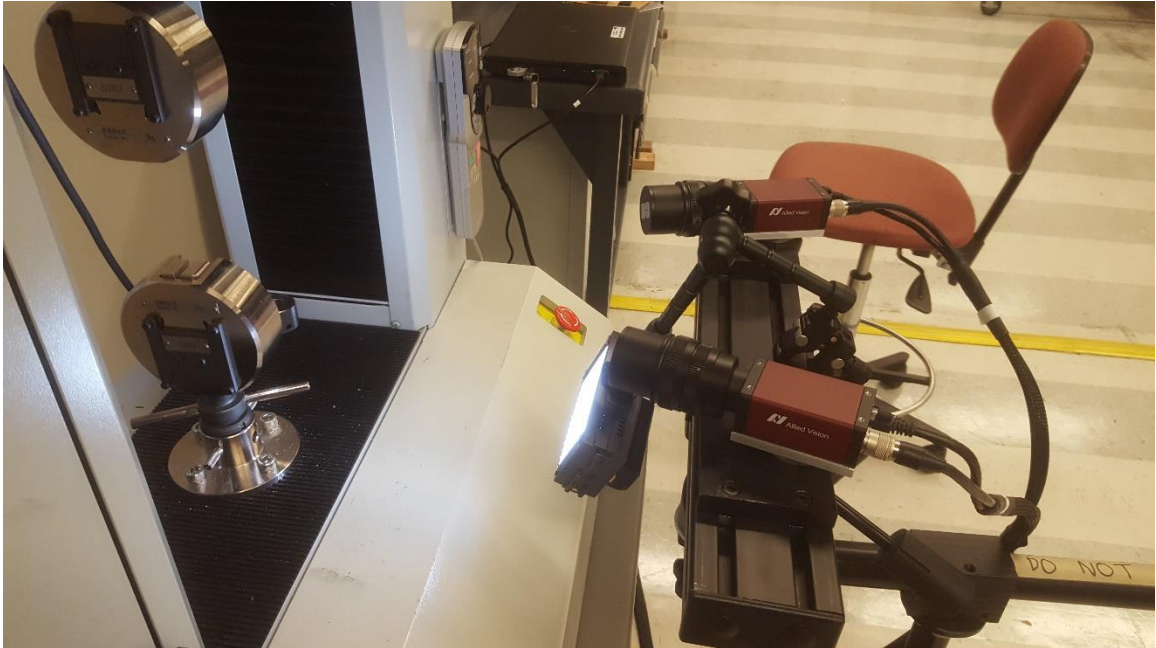


Figure 13: Test frame and 3D DIC setup



Figure 14: DCB sample being tested

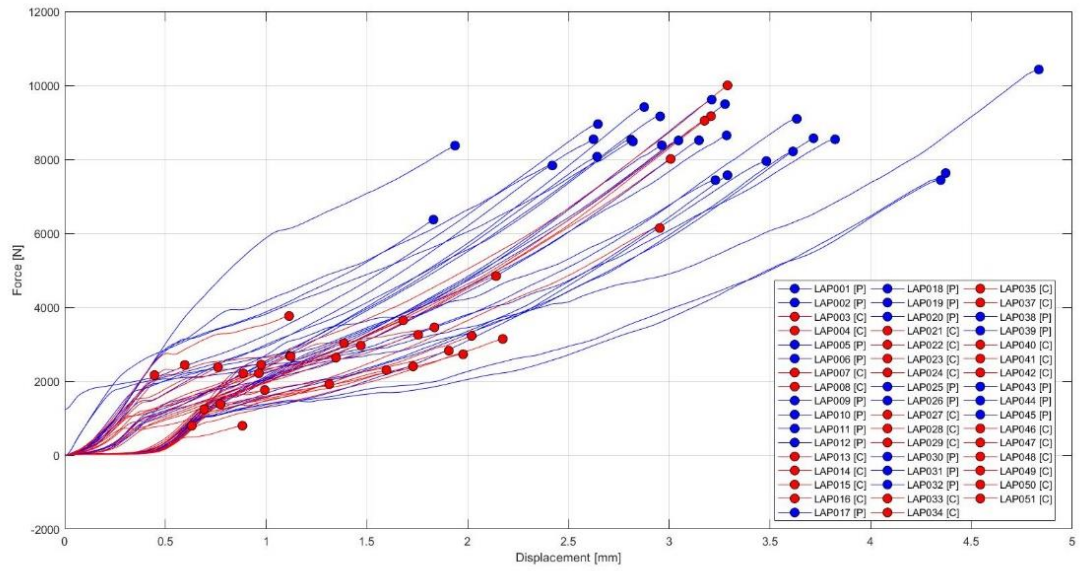


Figure 15: Material 1 normalized raw lap test data

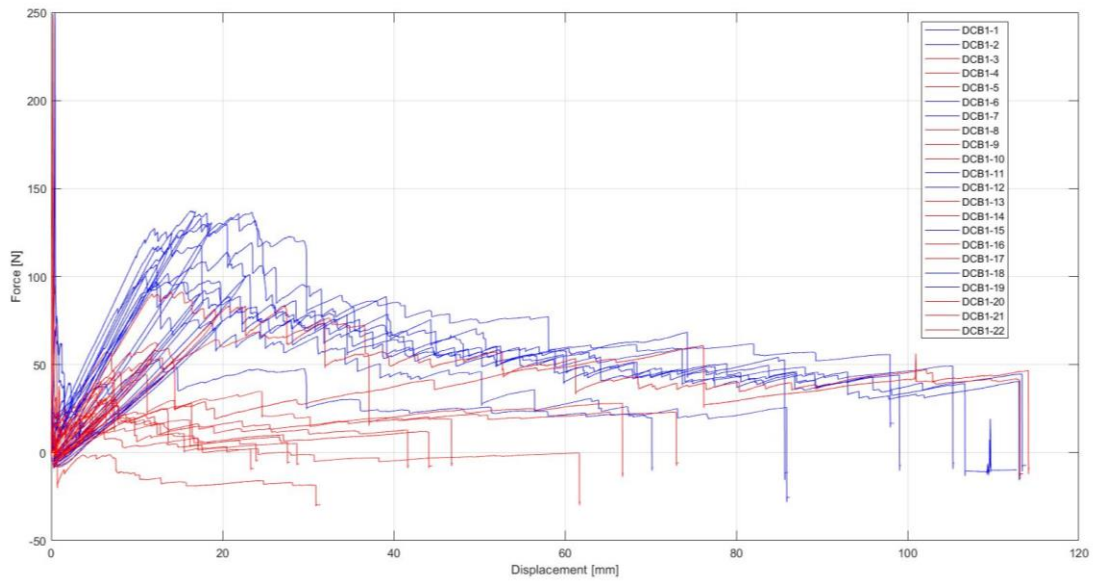


Figure 16: Material 1 normalized raw DCB test data

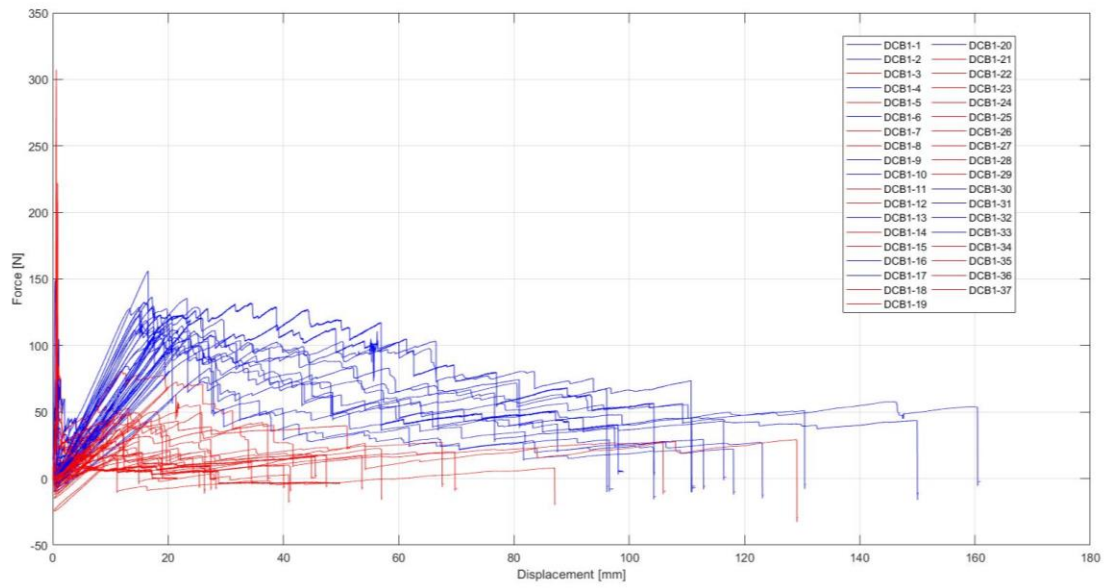


Figure 17: Material 2 normalized raw DCB test data

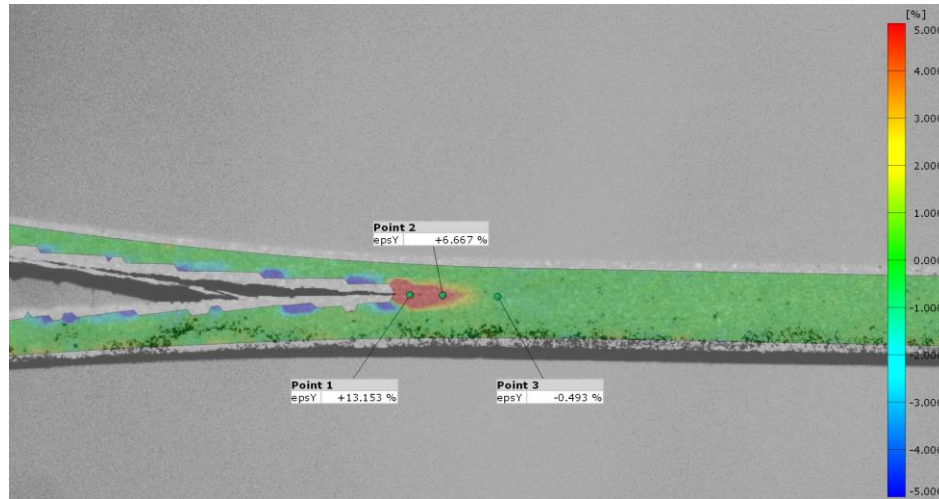


Figure 18: DIC image showing point and field strain measurement

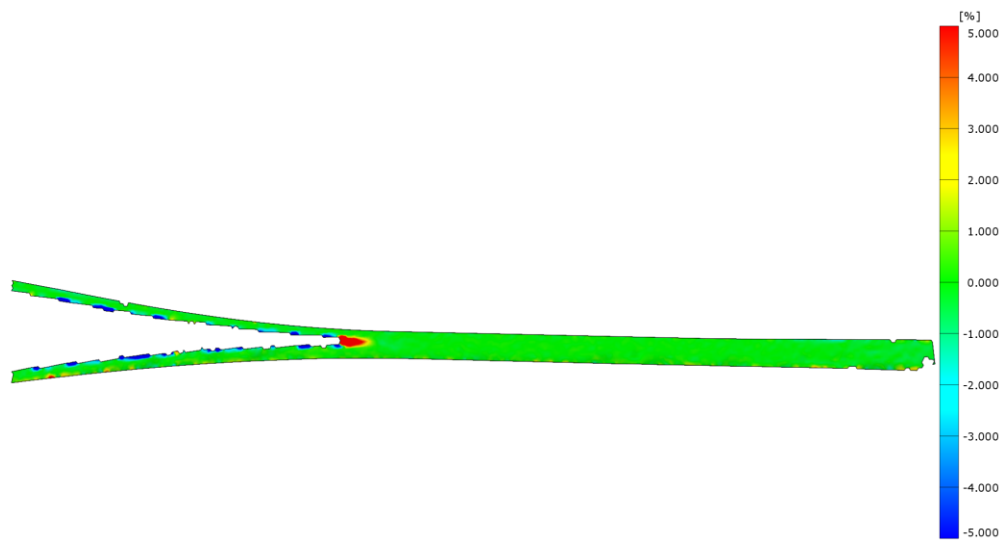


Figure 19: DIC image showing the surface mesh

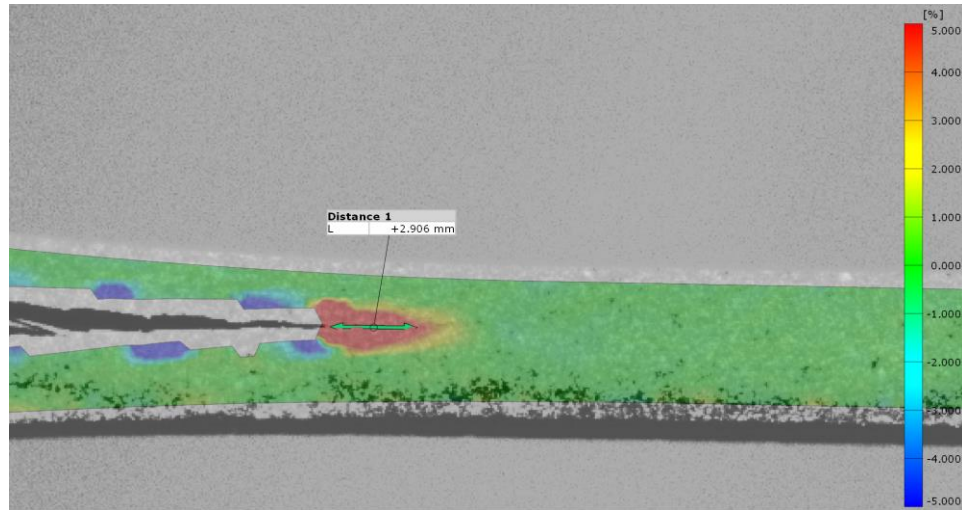


Figure 20: DIC image showing accurate distance measurement between two points

For the lap joint test, due to the geometry of the samples and the loading during the test, there was a mixed mode failure which can be modeled according to the Ojalvo and Eidinhoff [57]. They showed that there is substantial peel and shear stresses at the tips of the adhesive along the load axis. The failure stress was calculated under the assumption that the load was fully shear. The data shows that shear stress could be used to qualitatively compare the shear strength values, as stated by the ASTM D5868 standard [52]. Therefore, the shear stress at failure was simply used for the data comparison, but they cannot be used by itself to determine any underlying material properties.

The DCB peel test was used in order to find the Mode I initiation fracture toughness. The test was based on the ASTM D5528 standard [53]. The test performed was slightly modified from the ASTM standard for several reasons. First, the ASTM

standard was intended for use on unidirectional CFRP, while this test was used on a plain weave CFRP. Second, the ASTM observed only the interlaminar fracture toughness of only CFRP, while this test inserted an adhesive layer of two separate CFRP coupons. These differences may lead to less consistent results between samples, but the data reduction method used was the same. The fracture toughness was calculated using the modified beam theory (MBT). MBT was recommended in the ASTM standard because it was found to be the most conservative estimation method for the initiation fracture toughness. The equation used for calculating the Mode I fracture toughness can be seen in the equation below,

$$G_I = \frac{3P\delta}{2b(a+|\Delta|)}$$

where  $G_I$  is the fracture toughness,  $P$  is the load,  $\delta$  is the displacement,  $b$  is the specimen width,  $a$  is the delamination length, and  $\Delta$  is a correction factor that is determined experimentally for each sample. The load and displacement were both read from the load cell data. The specimen width was measured using calipers. The delamination length was measured using the DIC system. The correction factor is necessary because rotation may occur at the delamination front and can be corrected by treating the delamination as if it were longer [53]. The correction factor can be found by plotting the cube root of the compliance against the delamination length and then taking the x-intercept of the least squares plot as the correction factor. The compliance is simply the ratio of the load point displacement and the applied load. Once the correction factor is found, the initiation fracture toughness can be solved for.

The BTG Surface Analyst™ was used as a comprehensive measure of the surface quality by measuring the water contact angle. While not giving any data on any specific characteristic of the surface of the sample, the Surface Analyst was extremely valuable throughout the tests. The Surface Analyst uses purified water and a camera to record the water contact angle of the surface of the sample, as seen in Figure 21. In this research, the contact angles were very different in value between the pristine and contaminated samples. Though the contact angle is only a part of the information, due to its simplicity it can be a very efficient tool in analysis. Given a larger data set of samples, it is possible that the water contact angle could be used as a simple cut off point for the mechanic on the shop floor. Using the contact angle with this contaminant, the strong and very weak bonds could be easily differentiated.

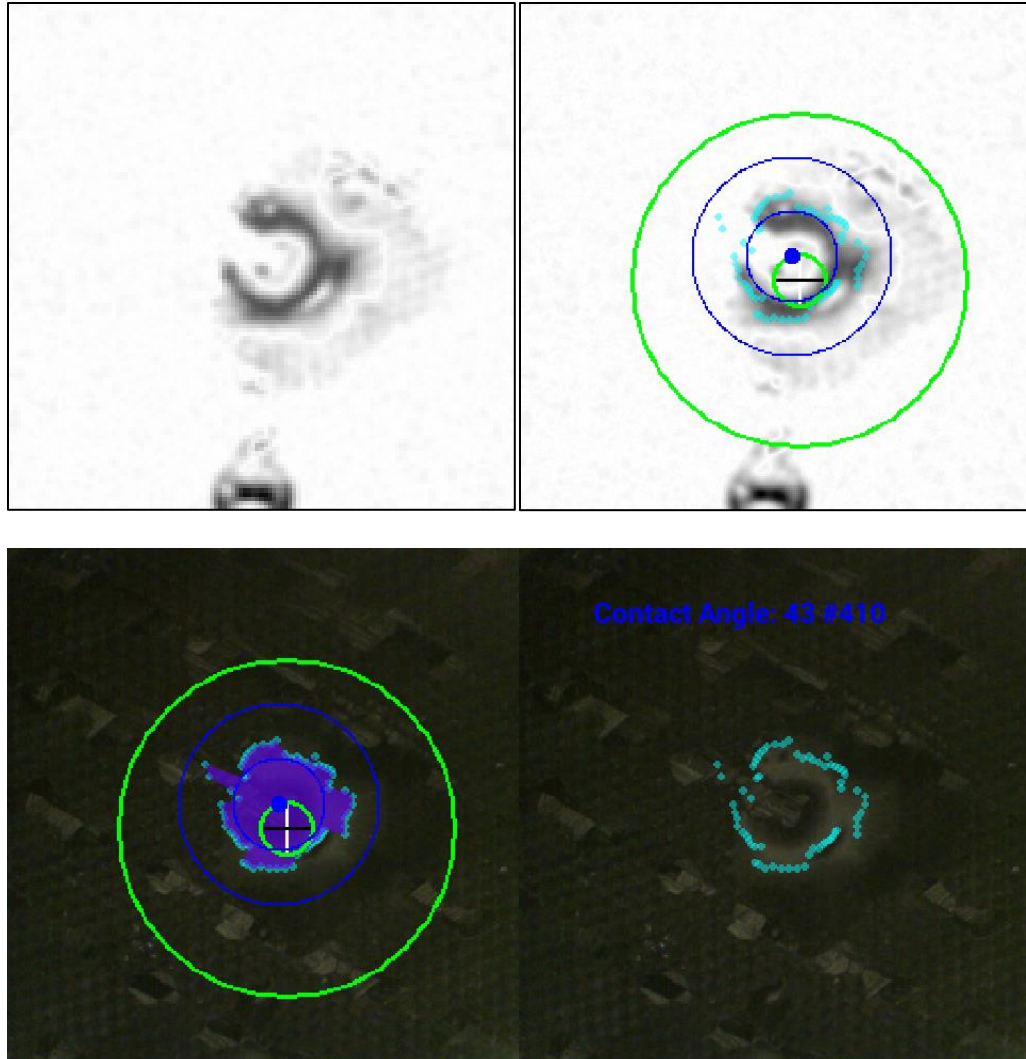


Figure 21: Surface Analyst contact angle images for higher contact angle

For this project, the Agilent Technologies 4300 Handheld FTIR was used initially to look at the surfaces of the samples after certain surface preparation methods and some contaminations. Some results examining the effect of sanding and isopropyl alcohol can be seen in Figure 22. Due to the nature of the handheld FTIR, the upward shift seen in the Sanded data is not important. There are no striking differences between the plots, which

may have to do with the isopropyl alcohol all evaporating or being absorbed into the substrate. FTIR was not used further in this project due to the knowledge of the chemical bonds required to interpret the data.

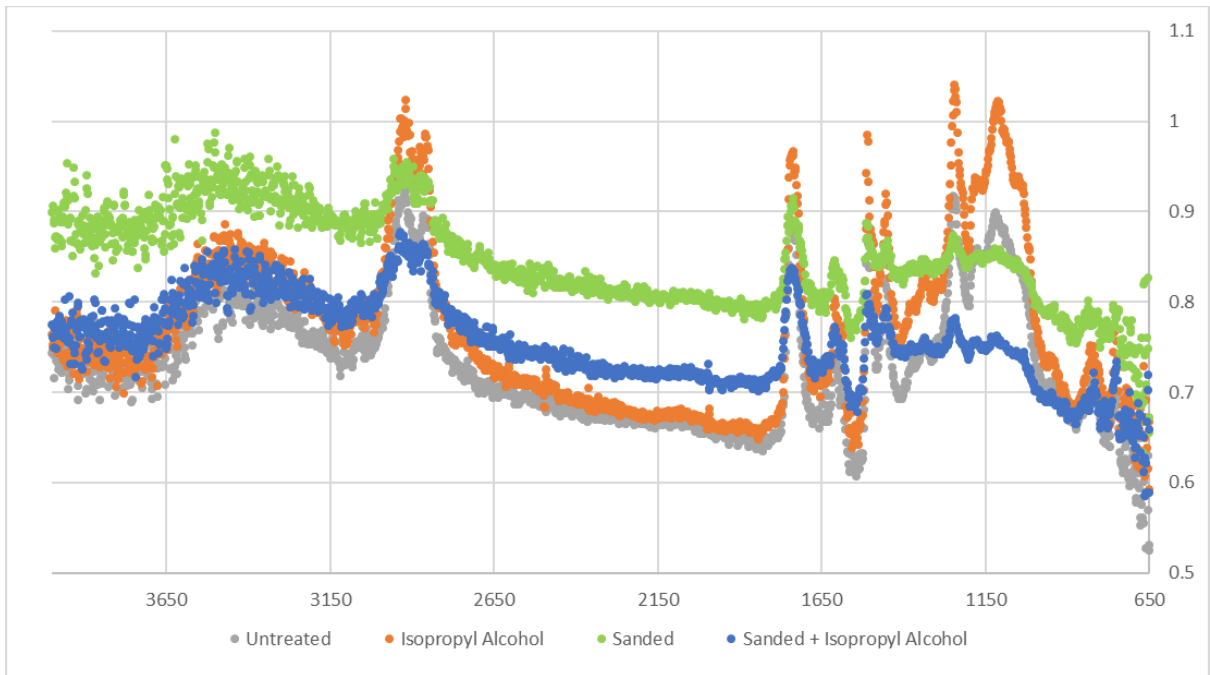


Figure 22: FTIR examination of sanding and isopropyl alcohol on Material 1

Another tool used in the lab is the KLA Tencor surface profiler. The surface profiler can measure the physical surface geometry of an area reliably on the micrometer scale. The surface profiler was used to compare sanded and unsanded surfaces of the Material 1 CFRP coupon. The unsanded and sanded surfaces can be seen in Figure 24-

Figure 26. In the unsanded scenario, there is a range in the height of the surface from about 55  $\mu\text{m}$ . The sanded sample, however, had a height range of 20  $\mu\text{m}$ . Future work could look at varying and studying the sanding method or grit. Beyond the initial investigation, there was no use of the surface profiler throughout the test. One reason for the lack of use is the amount of time to measure a small region on the samples. An area of 4  $\text{mm}^2$  would be measured over a period of 6 – 8 hours. Not only is this a large amount of time, but the data may not be representative of the rest of the surface of the sample.

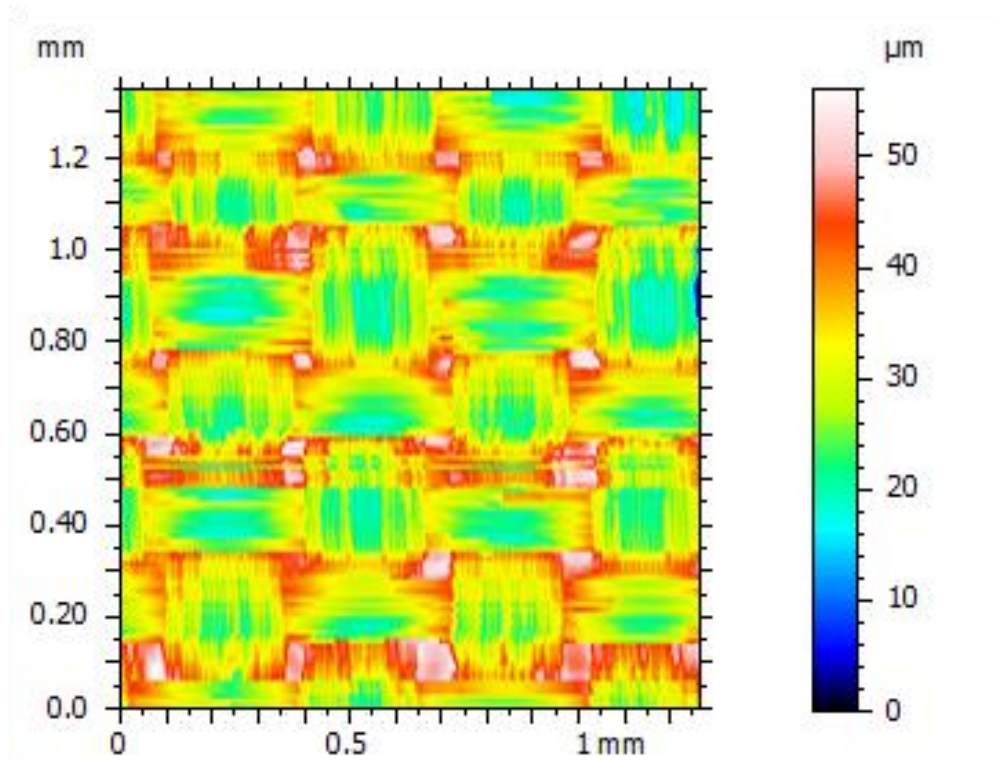


Figure 23: Unsanded Material 1 2D view of surface

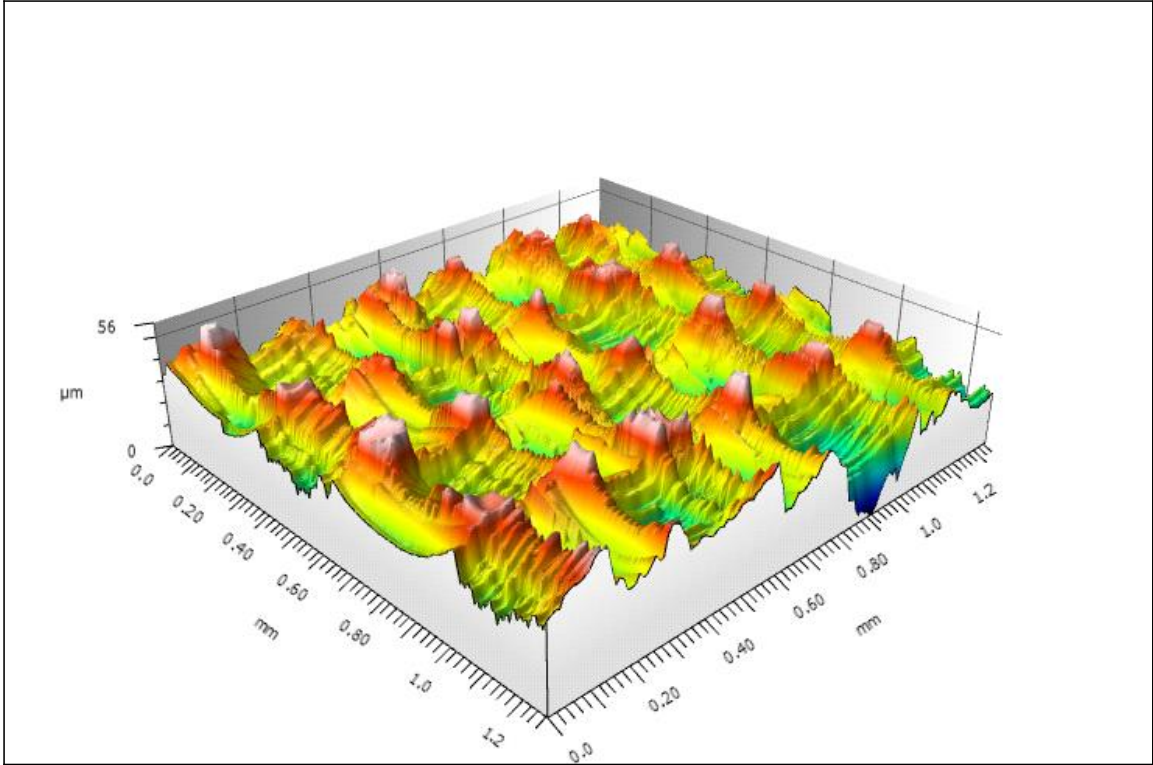


Figure 24: Unsanded Material 1 3D view of surface

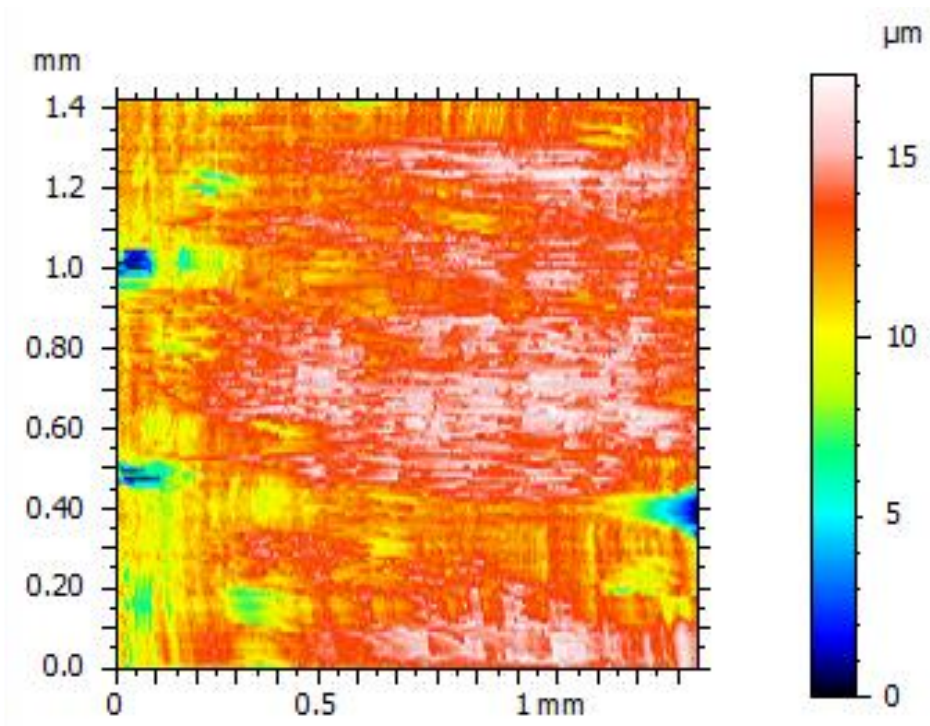


Figure 25: Sanded Material 1 2D view of surface

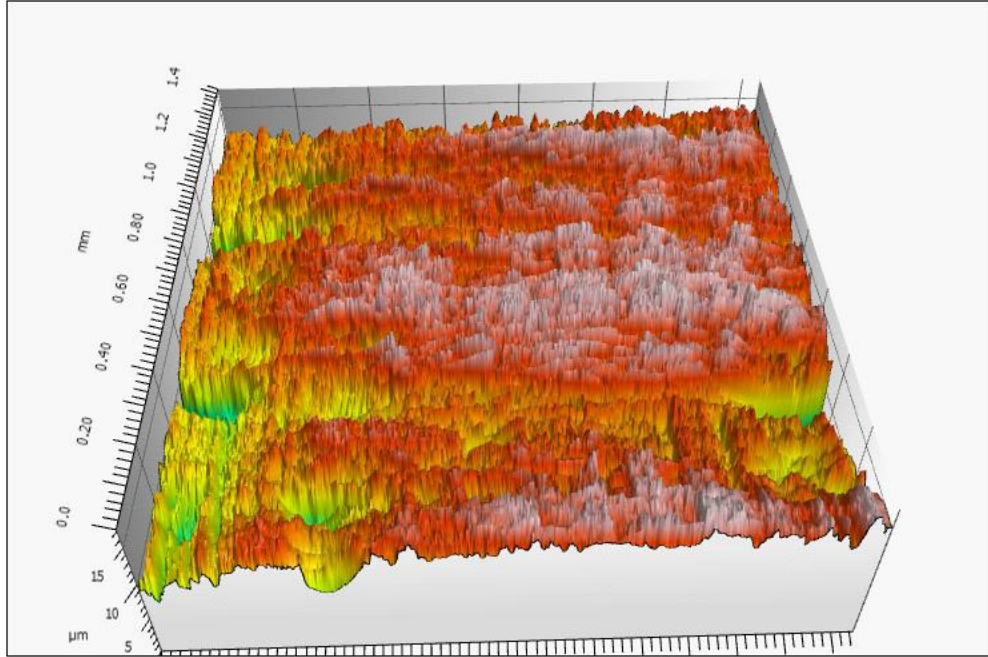


Figure 26: Sanded Material 1 3D view of surface

## RESULTS AND DISCUSSION

After testing the samples, the methods proved to be a reliable method of creating strong or weak bonded composite joints. The lap joint tests were found to be a good qualitative measure of the bond strength. There is more complexity in these series of tests than the basic fracture toughness calculation given in the ASTM D5528 standard can account for due to the adhesive and woven fabric CFRP. The complexity comes from the changing failure modes of crack propagation. The different failure modes can be seen in Figure 27 and Figure 28. The kissing bond corresponds to a total adhesive failure, while the other failure modes can happen in a strong bond. For each material and test, a similar trend was found between the contact angle and the bond strength, whether it be shear stress at failure or initiation fracture toughness.



(a)



(b)



(c)

Figure 27: Three failure modes, (a) adhesive, (b) adherend, and (c) cohesive

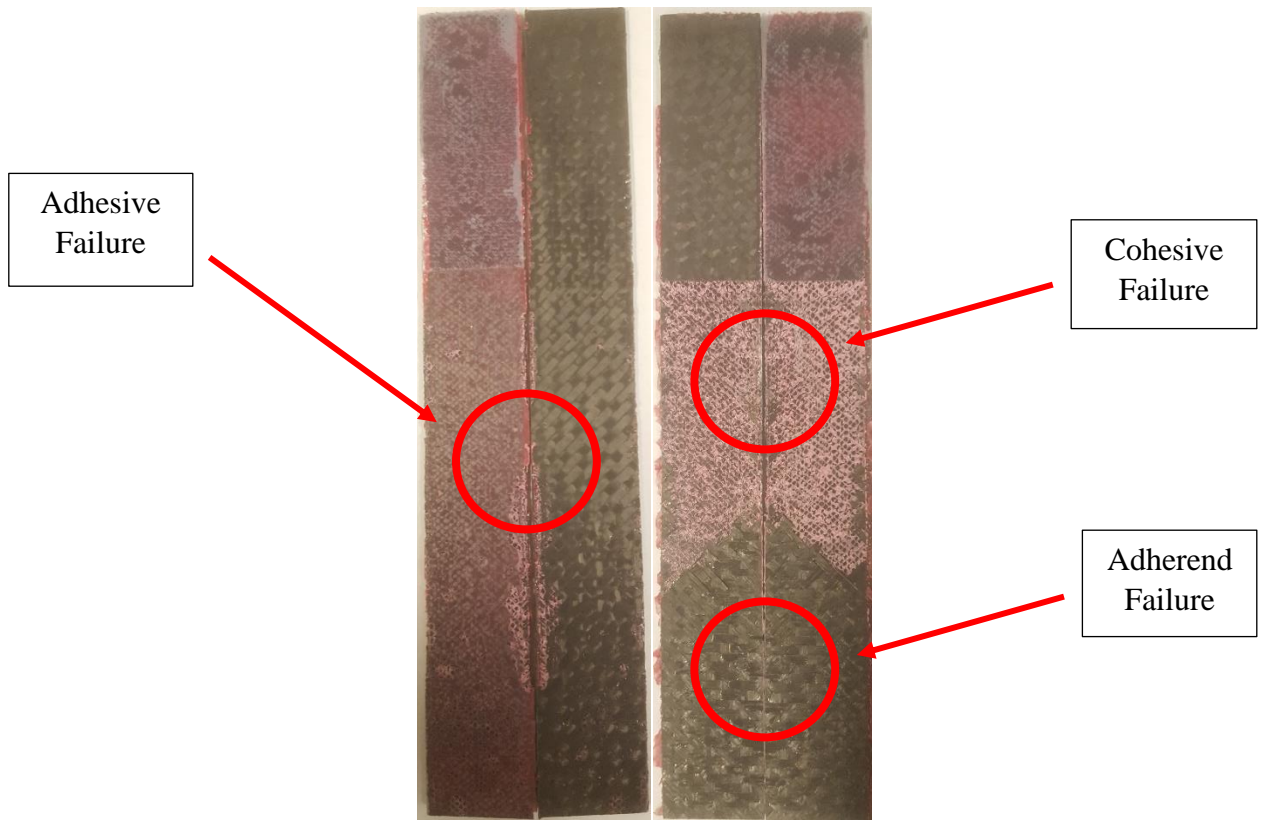


Figure 28: Failure modes on actual DCB sample

The lap test was performed on about 60 samples. The lap test failure stress and contact angles can be seen in Figure 29. Clearly, the water contact angle is not in and of itself a sufficient measure during fabrication for the failure stress. This is shown in the pristine sample results. Even though the pristine samples all have a very similar contact angle, the highest failure stress is roughly 50% larger than the smallest. A much greater variation is seen in the contaminated values. The average and standard deviation are shown in Figure 30. The average heavily contaminated failure stress is 32% of the

average pristine failure stress. This shows a large drop in failure stress for the contaminated samples. The normalized data table can be seen in Table 2 - Table 4.

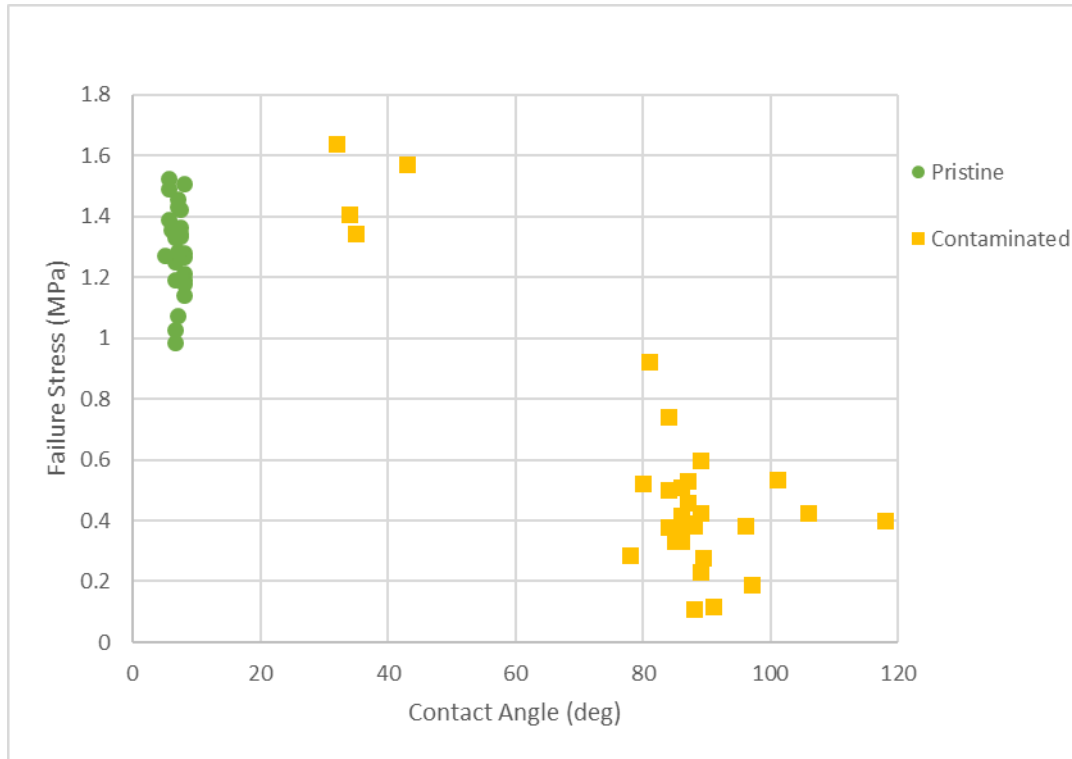


Figure 29: Material 1 lap joint failure stress plotted against contact angle

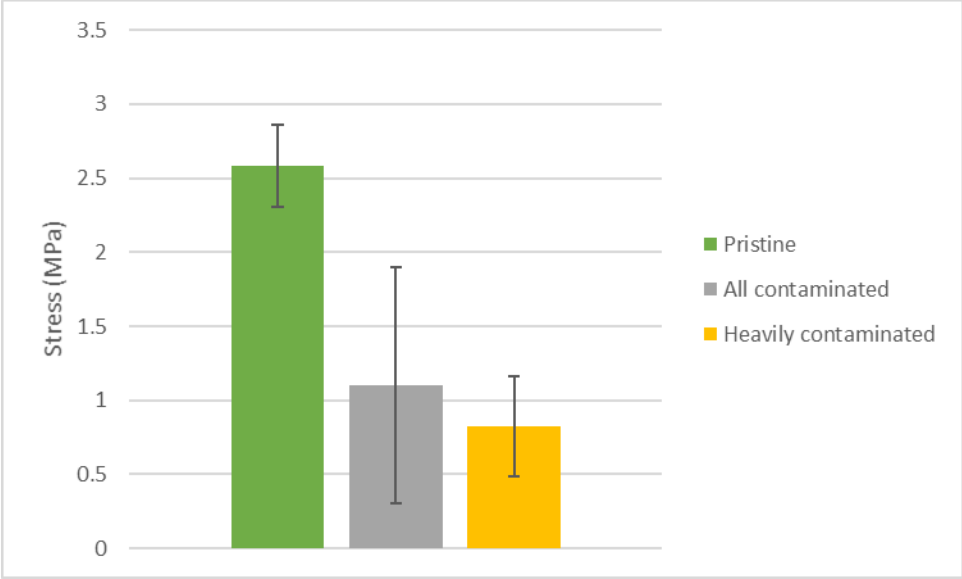


Figure 30: Normalized average failure stress for pristine, all, and heavily contaminated  
Material 1 lap joint samples

Table 2: Material 1 lap joint normalized data sample 1-20

Material 1	Layers	Film Out	Cure Temp.	Room Temp.	RH %	Sanded	Grit	Sand Method	SA (Deg.) A	SA (Deg.) B	Contam.	Contam. Type	Contam. SA (Deg.) A	Contam. SA (Deg.) B	Failure Modes	Kissing Bond	Break Stress (MPa)
LAP001	11	2	121	23.3	29	Y	220	H	7	9	N	N/A	N/A	N/A	ADHEREND; COHESIVE	N	2.180
LAP002	11	2	121	23.3	29	Y	220	H	8	6	N	N/A	N/A	N/A	ADHEREND; COHESIVE	N	1.827
LAP003	11	2	121	23.3	29	Y	220	H	6	6	Y	FG	29	34	ADHESIVE; COHESIVE	Y	0.682
LAP004	11	2	121	23.3	29	Y	220	H	5	5	Y	FG	49	27	ADHESIVE; COHESIVE	Y	0.762
LAP005	11	2.5	121	23.3	48.6	Y	220	H	6	7	N	N/A	N/A	N/A	ADHEREND; COHESIVE	N	1.749
LAP006	11	2.5	121	23.3	48.6	Y	220	H	6	7	N	N/A	N/A	N/A	ADHEREND; COHESIVE	N	2.129
LAP007	11	2.5	121	23.3	48.6	Y	220	H	7	6	Y	FK44NC	99	80	ADHESIVE; COHESIVE	Y	0.471
LAP008	11	2.5	121	23.3	48.6	Y	220	H	7	6	Y	FK44NC	79	77	ADHESIVE; COHESIVE	Y	0.489
LAP009	11	2.5	121	23.3	34	Y	220	H	7	7	N	N/A	N/A	N/A	ADHEREND; COHESIVE	N	2.477
LAP010	11	2.5	121	23.3	34	Y	220	H	6	6	N	N/A	N/A	N/A	ADHEREND; COHESIVE	N	2.305
LAP011	11	2.5	121	23.3	34	Y	220	H	6	8	N	N/A	N/A	N/A	ADHEREND; COHESIVE	N	2.438
LAP012	11	2.5	121	23.3	34	Y	220	H	5	6	N	N/A	N/A	N/A	ADHEREND; COHESIVE	N	2.589
LAP013	11	2.5	121	23.3	34	Y	220	H	7	7	Y	FK44NC	78	84	ADHESIVE; COHESIVE	Y	1.566
LAP014	11	2.5	121	23.3	34	Y	220	H	5	7	Y	FK44NC	82	86	ADHESIVE	Y	0.854
LAP015	11	2.5	121	23.3	34	Y	220	H	7	5	Y	FK44NC	84	N/A	ADHESIVE	Y	1.262
LAP016	11	2.5	121	23.3	34	Y	220	H	6	5	Y	HENKEL	89	N/A	ADHESIVE	Y	1.014
LAP017	11	2.5	121	18.8	64.4	Y	220	H	8	7	N	N/A	N/A	N/A	ADHEREND; COHESIVE	N	2.272
LAP018	11	2.5	121	18.8	64.4	Y	220	H	6	7	N	N/A	N/A	N/A	ADHEREND; COHESIVE	N	1.675
LAP019	11	2.5	121	18.8	64.4	Y	220	H	6	8	N	N/A	N/A	N/A	ADHEREND; COHESIVE	N	2.160
LAP020	11	2.5	121	18.8	64.4	Y	220	H	7	8	N	N/A	N/A	N/A	ADHEREND; COHESIVE	N	2.419

Table 3: Material 1 lap joint normalized DCB data samples 21-40

Material 1	Layers	Film Out	Cure Temp.	Room Temp.	RH %	Sanded	Grit	Sand Method	SA (Deg.) A	SA (Deg.) B	Contam.	Contam. Type	Contam. SA (Deg.) A	Contam. SA (Deg.) B	Failure Modes	Kissing Bond	Break Stress (MPa)
	LAP021	11	2.5	121	18.8	64.4	Y	220	H	7	6	Y	FK44NC	43	N/A	MIXED/COHESIVE	N
LAP022	11	2.5	121	18.8	64.4	Y	220	H	9	7	Y	FK44NC	34	N/A	MIXED/COHESIVE	N	2.394
LAP023	11	2.5	121	18.8	64.4	Y	220	H	7	8	Y	FK44NC	32	N/A	MIXED/COHESIVE	N	2.785
LAP024	11	2.5	121	18.8	64.4	Y	220	H	8	7	Y	FK44NC	35	N/A	MIXED/COHESIVE	N	2.281
LAP025	11	3.5	121	19.3	63	Y	220	H	5	6	N	N/A	N/A	N/A	ADHEREND; COHESIVE	N	2.366
LAP026	11	3.5	121	19.3	63	Y	220	H	6	4	N	N/A	N/A	N/A	ADHEREND; COHESIVE	N	2.162
LAP027	11	3.5	121	19.3	63	Y	220	H	7	7	Y	FK44NC	N/A	118	ADHESIVE	Y	0.679
LAP028	11	3.5	121	19.3	63	Y	220	H	7	5	Y	FK44NC	N/A	101	ADHESIVE; COHESIVE	Y	0.910
LAP029	11	3.5	121	19.3	63	Y	220	H	6	6	Y	FK44NC	N/A	106	ADHESIVE	Y	0.723
LAP030	11	5.5	121	19.3	62	Y	220	H	6	7	N	N/A	N/A	N/A	ADHEREND; COHESIVE	N	2.029
LAP031	11	5.5	121	19.3	62	Y	220	H	8	8	N	N/A	N/A	N/A	ADHEREND; COHESIVE	N	2.062
LAP032	11	5.5	121	19.3	61.5	Y	220	H	8	8	N	N/A	N/A	N/A	ADHEREND; COHESIVE	N	2.029
LAP033	11	5.5	121	19.3	61.5	Y	220	H	8	7	Y	FK44NC	N/A	89	ADHESIVE	Y	0.390
LAP034	11	5.5	121	19.3	61.5	Y	220	H	8	8	Y	FK44NC	N/A	97	ADHESIVE	Y	0.326
LAP035	11	5.5	121	19.3	61.5	Y	220	H	8	7	Y	FK44NC	N/A	88	ADHESIVE	Y	0.189
LAP036	11	5.5	121	19.3	61.5	Y	220	H	7	8	Y	FK44NC	N/A	87	ADHESIVE	Y	0.000
LAP037	11	5.5	121	19.3	61.5	Y	220	H	8	7	Y	FK44NC	N/A	91	ADHESIVE	Y	0.201
LAP038	11	5.5	121	19.3	61.5	Y	220	H	6	5	N	N/A	N/A	N/A	ADHEREND; COHESIVE	N	2.535
LAP039	11	5.5	121	19.3	61.5	Y	220	H	8	8	N	N/A	N/A	N/A	ADHEREND; COHESIVE	N	2.152
LAP040	11	5.5	121	19.3	61.5	Y	220	H	8	7	Y	FK44NC	N/A	89	ADHESIVE	Y	0.726

Table 4: Material 1 lap joint normalized data sample 41-60

Material 1	Layers	Film Out	Cure Temp.	Room Temp.	RH %	Sanded	Grit	Sand Method	SA (Deg.) A	SA (Deg.) B	Contam.	Contam. Type	Contam. SA (Deg.) A	Contam. SA (Deg.) B	Failure Modes	Kissing Bond	Break Stress (MPa)
LAP041	11	5.5	121	19.3	61.5	Y	220	H	7	5	Y	FK44NC	N/A	86	ADHESIVE	Y	0.628
LAP042	11	5.5	121	19.3	61.5	Y	220	H	6	7	Y	FK44NC	N/A	96	ADHESIVE	Y	0.652
LAP043	11	5.5	121	19.5	50.4	Y	220	H	6	7	N	N/A	N/A	N/A	ADHEREND; COHESIVE	N	2.261
LAP044	11	5.5	121	19.5	50.4	Y	220	H	7	8	N	N/A	N/A	N/A	ADHEREND; COHESIVE	N	2.322
LAP045	11	5.5	121	19.5	50.4	Y	220	H	8	7	N	N/A	N/A	N/A	ADHEREND; COHESIVE	N	2.287
LAP046	11	5.5	121	19.5	50.4	Y	220	H	7	7	Y	FK44NC	N/A	87	ADHESIVE	Y	0.669
LAP047	11	5.5	121	19.5	50.4	Y	220	H	7	7	Y	FK44NC	N/A	87	ADHESIVE	Y	0.903
LAP048	11	5.5	121	19.5	50.4	Y	220	H	7	8	Y	FK44NC	N/A	86	ADHESIVE	Y	0.709
LAP049	11	5.5	121	19.5	50.4	Y	220	H	8	7	Y	FK44NC	N/A	87	ADHESIVE	Y	0.779
LAP050	11	5.5	121	19.5	50.4	Y	220	H	7	7	Y	FK44NC	N/A	86	ADHESIVE	Y	0.562
LAP051	11	5.5	121	19.5	50.4	Y	220	H	7	7	Y	FK44NC	N/A	86	ADHESIVE	Y	0.867
LAP052	11	5.5	121	19.5	50.4	Y	220	H	7	7	Y	FK44NC	N/A	88	ADHESIVE	Y	0.648
LAP053	11	7	121	19.5	45	Y	220	H	8	8	N	N/A	N/A	N/A	ADHEREND; COHESIVE	N	1.941
LAP054	11	7	121	19.5	45	Y	220	H	8	8	N	N/A	N/A	N/A	ADHEREND; COHESIVE	N	2.002
LAP055	11	5.5	121	19.5	45	Y	220	H	8	8	Y	FK44NC	N/A	84	ADHESIVE	Y	0.647
LAP056	11	5.5	121	19.5	45	Y	220	H	9	9	Y	FK44NC	N/A	86	ADHESIVE	Y	0.574
LAP057	11	7	121	19.5	45	Y	220	H	7	7	N	N/A	N/A	N/A	ADHEREND; COHESIVE	N	2.184
LAP058	11	7	121	19.5	45	Y	220	H	7	9	N	N/A	N/A	N/A	ADHEREND; COHESIVE	N	2.562
LAP059	11	5.5	121	19.5	45	Y	220	H	9	8	Y	FK44NC	N/A	85	ADHESIVE	Y	0.568
LAP060	11	5.5	121	19.5	45	Y	220	H	9	8	Y	FK44NC	N/A	80	ADHESIVE	Y	0.886

There was one batch of less contaminated samples which have a contact angles between 30° and 60° of Figure 29. The focus of these tests was on the highly contaminated and pristine cases. One batch was tested with less contaminant, and therefore a lower contact angle. Though these less contaminated samples had a failure stress similar to that of pristine samples, there was still a difference in the failure stress between the pristine and heavily contaminated samples. Future work could look at the intermediate values of the contact angle with more data. The difference between including all contaminated samples and just the heavily contaminated samples in the

average and standard deviation data can be seen in Figure 30. The clear difference between the pristine and heavily contaminated samples is useful for NDI tests to have the most remarkable differences between contaminated samples.

The DCB samples had similar trends to the lap joint samples for Material 1. In Figure 31 we see the DCB fracture toughness results plotted against the contact angle. The similar trend between the Material 1 DCB fracture toughness, Figure 31, and the lap joints failure stress, Figure 29, are apparent. The average values and standard deviation of the initiation fracture toughness for the Material 1 DCB test can be seen in Figure 32. The average contaminated initiation fracture toughness is 13% of the average pristine initiation fracture toughness. Once again there is a large difference between the pristine and heavily contaminated cases. The normalized data table for these samples can be seen in Table 5.

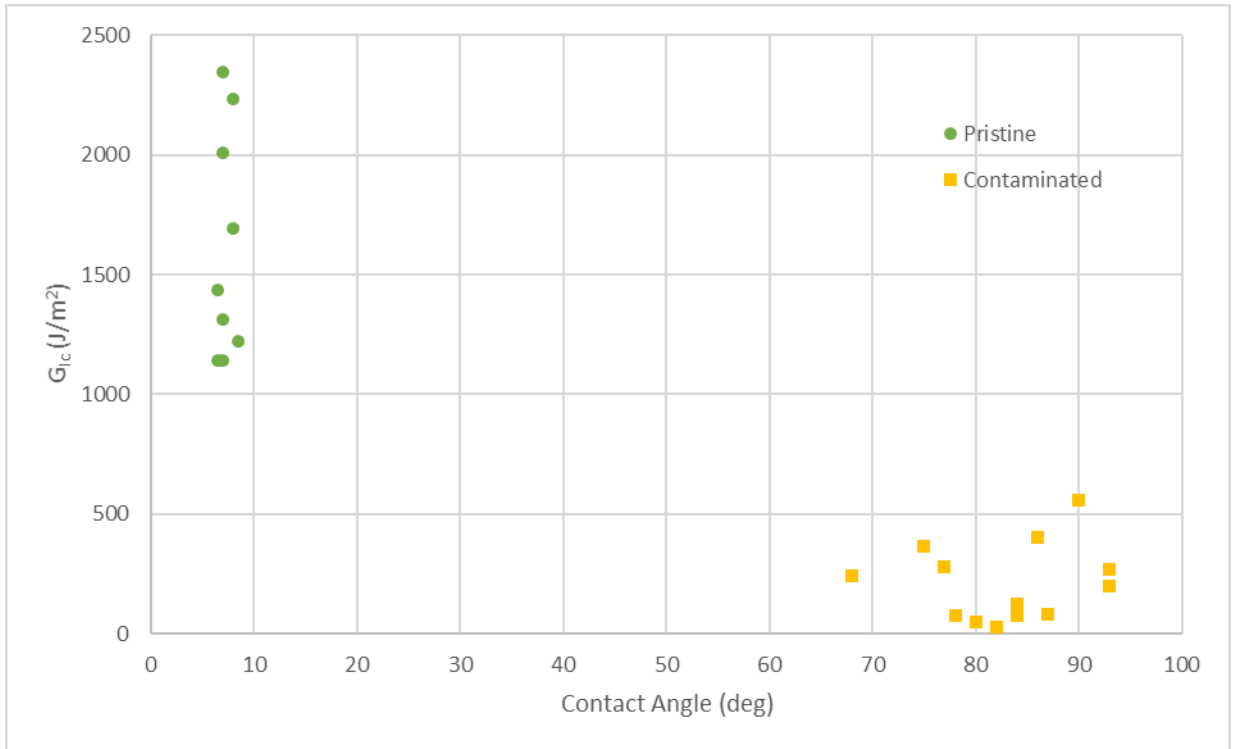


Figure 31: Material 1 normalized DCB fracture toughness plotted against contact angle

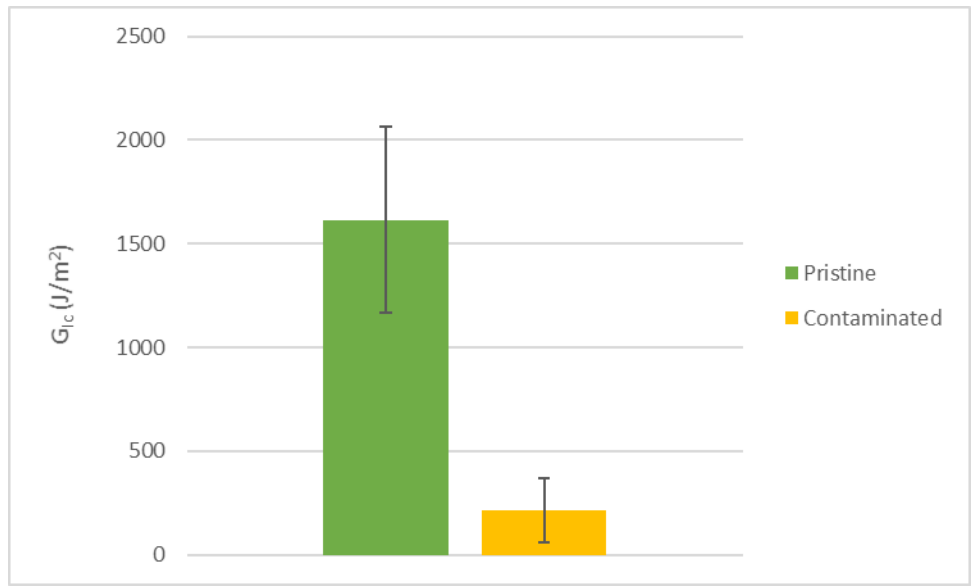


Figure 32: Material 1 normalized pristine and contaminated DCB average fracture toughness

Table 5: Material 1 normalized DCB data sample

Material 1	Layers	Film Out	Cure Temp.	Room Temp.	RH %	Sanded	Grit	Sand Method	SA (Deg.) A	SA (Deg.) B	Contam.	Contam. Type	Contam. SA (Deg.) A	Contam. SA (Deg.) B	Failure Modes	Kissing Bond	Initiation Fracture Toughness (J/m <sup>2</sup> )
DCB1-1	11	5	121	19.3	63	Y	220	H	8	8	N	N/A	N/A	N/A	COHESIVE/ADHEREND	N	1465.54
DCB1-2	11	5	121	19.3	63	Y	220	H	7	7	N	N/A	N/A	N/A	COHESIVE/ADHEREND	N	2030.91
DCB1-3	11	5	121	19.3	63	Y	220	H	7	7	Y	FK44NC	N/A	80	ADHESIVE	Y	43.94
DCB1-4	11	5	121	19.3	63	Y	220	H	7	8	Y	FK44NC	N/A	84	ADHESIVE	Y	109.44
DCB1-5	11	5	121	19.3	63	Y	220	H	8	8	Y	FK44NC	N/A	86	ADHESIVE	Y	349.09
DCB1-6	11	5.5	121	19.3	61.6	Y	220	H	7	6	N	N/A	N/A	N/A	COHESIVE/ADHEREND	N	991.46
DCB1-7	11	5.5	121	19.3	61.6	Y	220	H	6	8	N	N/A	N/A	N/A	COHESIVE/ADHEREND	N	990.80
DCB1-8	11	5.5	121	19.3	61.6	Y	220	H	7	8	Y	FK44NC	N/A	82	ADHESIVE	Y	26.04
DCB1-9	11	5.5	121	19.3	61.6	Y	220	H	8	8	Y	FK44NC	N/A	84	ADHESIVE	Y	67.12
DCB1-10	11	5.5	121	19.3	61.6	Y	220	H	6	6	Y	FK44NC	N/A	87	ADHESIVE	Y	71.82
DCB1-11	11	5.5	121	19.6	62.3	Y	220	H	5	8	N	N/A	N/A	N/A	COHESIVE/ADHEREND	N	1243.81
DCB1-12	11	5.5	121	19.6	62.3	Y	220	H	7	7	N	N/A	N/A	N/A	COHESIVE/ADHEREND	N	1135.78
DCB1-13	11	5.5	121	19.6	62.3	Y	220	H	7	8	Y	FK44NC	N/A	93	ADHESIVE	Y	175.03
DCB1-14	11	5.5	121	19.6	62.3	Y	220	H	8	7	Y	FK44NC	N/A	93	ADHESIVE	Y	233.55
DCB1-15	11	7	121	19.3	18.3	Y	220	H	7	7	N	N/A	N/A	N/A	ADHEREND	N	1740.33
DCB1-16	11	7	121	19.3	18.3	Y	220	H	7	7	Y	FK44NC	N/A	78	ADHESIVE	Y	65.02
DCB1-17	11	7	121	19.3	18.3	Y	220	H	7	7	Y	FK44NC	N/A	77	ADHESIVE	Y	241.38
DCB1-18	11	22	121	19.1	60.2	Y	220	H	9	7	N	N/A	N/A	N/A	COHESIVE/ADHEREND	N	1936.91
DCB1-19	11	22	121	19.1	60.2	Y	220	H	8	9	N	N/A	N/A	N/A	COHESIVE/ADHEREND	N	1056.69
DCB1-20	11	22	121	19.1	60.2	Y	220	H	8	8	Y	FK44NC	N/A	75	ADHESIVE	Y	316.98
DCB1-21	11	22	121	19.1	60.2	Y	220	H	8	9	Y	FK44NC	N/A	68	ADHESIVE	Y	210.42
DCB1-22	11	9.3	121	19.2	61.4	Y	220	H	8	8	Y	FK44NC	N/A	90	ADHESIVE/ADHEREND	Y	485.14

The Material 2 samples failed with a similar trend to the Material 1 material and lap joint test. The initiation fracture toughness value and contact angle plot can be seen in Figure 33. The average contaminated initiation fracture toughness is 11% of the pristine initiation fracture toughness. Again, there is a large spread between the pristine samples in their fracture toughness values, with the highest being more than twice as high of the lowest, with a small range of contact angle between 6° and 10°. For all of the tests, the contact angle is not enough information in and of itself to reliably predict the bond

strength. This is why the other fabrication data is important. The contact angle likely does not take in important information such as the humidity, material out-time, or any in-situ factors during curing of the prepreg. Any information about the in-situ curing of the adhesive certainly cannot be extracted from the contact angle because it is impossible to use the contact angle on the bonded region once the curing has begun. The normalized data table can be seen in Table 6 and Table 7.

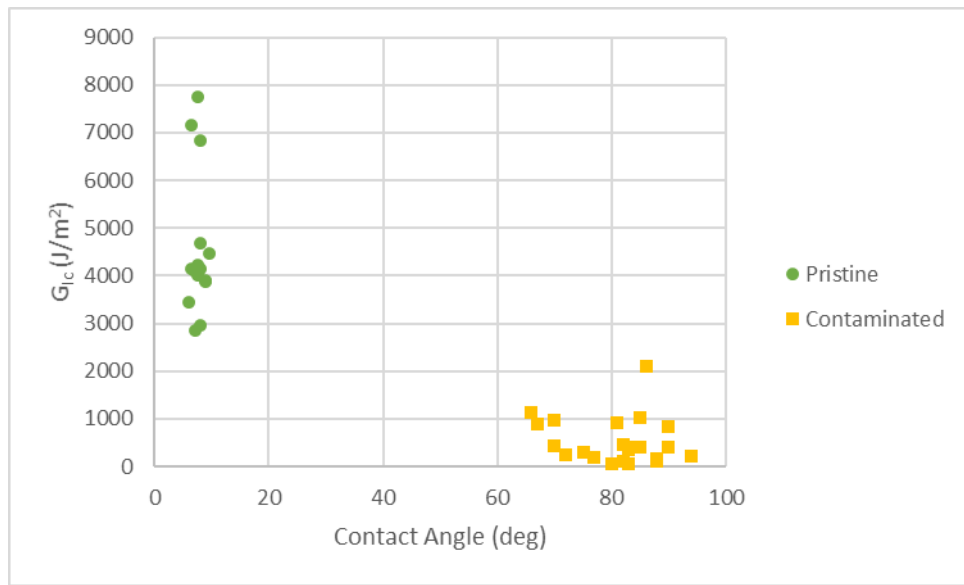


Figure 33: Material 2 DCB normalized fracture toughness plotted against contact angle

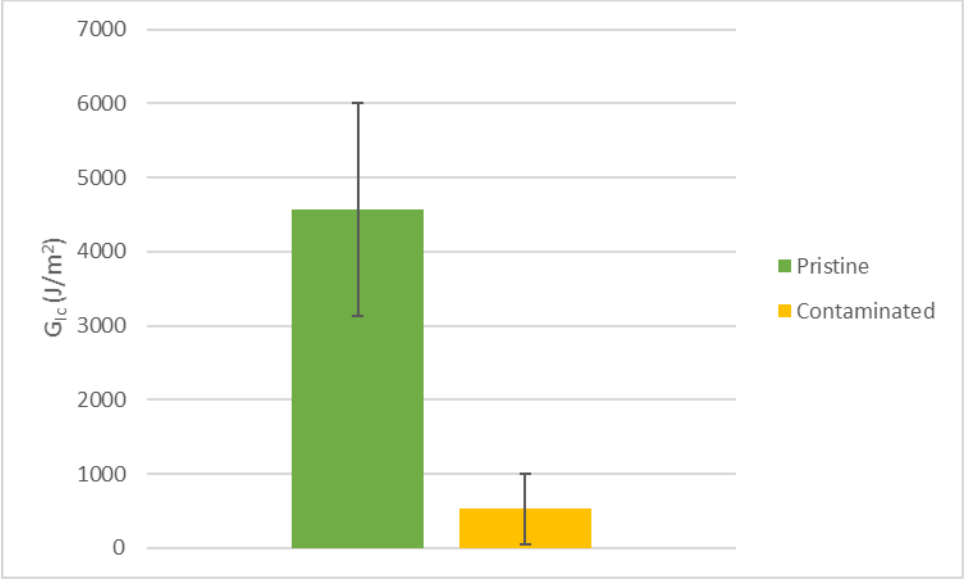


Figure 34: Material 2 normalized pristine and contaminated DCB average fracture toughness

Table 6: Material 2 normalized DCB data samples 1-20

Material 2	Layers	Film Out	Cure Temp.	Room Temp.	RH %	Sanded	Grit	Sand Method	SA (Deg.) A	SA (Deg.) B	Contam.	Contam. Type	Contam. SA (Deg.) A	Contam. SA (Deg.) B	Failure Modes	Kissing Bond	Initiation Fracture Toughness (J/m <sup>2</sup> )
	DCB2-1	11	4.5	121	18.4	66	Y	220	H	7	6	N	N/A	N/A	N/A	ADHEREND	N
DCB2-2	11	4.5	121	18.4	66	Y	220	H	8	7	N	N/A	N/A	N/A	COHESIVE/ADHEREND	N	743
DCB2-3	11	5	121	19.1	66	Y	220	H	8	6	N	N/A	N/A	N/A	COHESIVE/ADHEREND	N	528
DCB2-4	11	5	121	19.1	66	Y	220	H	6	6	N	N/A	N/A	N/A	COHESIVE/ADHEREND	N	637
DCB2-5	11	5	121	19.1	66	Y	220	H	6	7	Y	FK44NC	N/A	77	ADHESIVE	Y	34
DCB2-6	11	5	121	19.1	66	Y	220	H	5	7	Y	FK44NC	N/A	75	ADHESIVE	Y	54
DCB2-7	11	5.5	121	19.6	62.3	Y	220	H	7	6	N	N/A	N/A	N/A	ADHEREND	N	1325
DCB2-8	11	5.5	121	19.6	62.3	Y	220	H	8	8	N	N/A	N/A	N/A	ADHEREND	N	1268
DCB2-9	11	5.5	121	19.6	62.3	Y	220	H	7	8	Y	FK44NC	N/A	94	ADHESIVE	Y	38
DCB2-10	11	5.5	121	19.6	62.3	Y	220	H	8	7	Y	FK44NC	N/A	90	ADHESIVE	Y	73
DCB2-11	11	7	121	19.3	18.3	Y	220	H	7	7	N	N/A	N/A	N/A	COHESIVE/ADHEREND	N	#VALUE!
DCB2-12	11	7	121	19.3	18.3	Y	220	H	8	8	Y	FK44NC	N/A	72	ADHESIVE	Y	44
DCB2-13	11	7	121	19.3	18.3	Y	220	H	7	8	Y	FK44NC	N/A	70	ADHESIVE	Y	80
DCB2-14	11	23	121	18.9	26.4	Y	220	O	7	8	N	N/A	N/A	N/A	COHESIVE/ADHEREND	N	869
DCB2-15	11	23	121	18.9	26.4	Y	220	O	7	9	N	N/A	N/A	N/A	COHESIVE/ADHEREND	N	719
DCB2-16	11	23	121	18.9	26.4	Y	220	O	8	7	Y	FK44NC	N/A	67	ADHESIVE	Y	163
DCB2-17	11	23	121	18.9	26.4	Y	220	O	7	9	Y	FK44NC	N/A	66	ADHESIVE	Y	212
DCB2-18	11	23	121	19.1	49.7	Y	120	O	7	8	N	N/A	N/A	N/A	COHESIVE/ADHEREND	N	546
DCB2-19	11	23	121	19.1	49.7	Y	120	O	8	8	Y	FK44NC	N/A	85	ADHESIVE	Y	192
DCB2-20	11	23	121	19.1	49.7	Y	120	O	9	8	Y	FK44NC	N/A	86	ADHESIVE/COHESIVE	Y	391

Table 7: Material 2 normalized DCB data sample 21-37

Material 2	Layers	Film Out	Cure Temp.	Room Temp.	RH %	Sanded	Grit	Sand Method	SA (Deg.) A	SA (Deg.) B	Contam.	Contam. Type	Contam. SA (Deg.) A	Contam. SA (Deg.) B	Failure Modes	Kissing Bond	Initiation Fracture Toughness (J/m <sup>2</sup> )
DCB2-21	11	23	121	19.1	49.7	Y	120	O	8	7	Y	FK44NC	N/A	81	ADHESIVE	Y	168
DCB2-22	11	23	121	19.1	49.7	Y	120	O	8	7	Y	FK44NC	N/A	90	ADHESIVE	Y	155
DCB2-23	11	23	121	19.1	49.7	Y	120	O	8	8	Y	FK44NC	N/A	70	ADHESIVE/COHESIVE	Y	178
DCB2-24	11	23	121	19.1	49.7	Y	120	O	8	8	Y	FK44NC	N/A	85	ADHESIVE/COHESIVE	Y	76
DCB2-25	11	23	121	19.1	49.7	Y	120	O	9	8	Y	FK44NC	N/A	83	ADHESIVE	Y	10
DCB2-26	11	24	121	18.9	63.2	Y	120	O	7	7	N	N/A	N/A	N/A	COHESIVE/ADHEREND	N	759
DCB2-27	11	24	121	18.9	63.2	Y	120	O	7	8	N	N/A	N/A	N/A	COHESIVE/ADHEREND	N	782
DCB2-28	11	24	121	18.9	63.2	Y	120	O	8	8	Y	FK44NC	N/A	82	ADHESIVE	Y	19
DCB2-29	11	24	121	18.9	63.2	Y	120	O	7	7	Y	FK44NC	N/A	88	ADHESIVE	Y	19
DCB2-30	11	24	121	18.9	63.2	Y	120	O	7	7	Y	FK44NC	N/A	88	ADHESIVE	Y	29
DCB2-31	11	24	121	18.9	63.2	Y	120	O	7	7	Y	FK44NC	N/A	80	ADHESIVE	Y	11
DCB2-32	11	22	121	19.1	62.6	Y	120	O	10	9	N	N/A	N/A	N/A	COHESIVE/ADHEREND	N	826
DCB2-33	11	22	121	19.1	62.6	Y	120	O	9	9	N	N/A	N/A	N/A	COHESIVE/ADHEREND	N	725
DCB2-34	11	22	121	19.1	62.6	Y	120	O	10	9	Y	FK44NC	N/A	83	ADHESIVE	Y	66
DCB2-35	11	22	121	19.1	62.6	Y	120	O	9	10	Y	FK44NC	N/A	84	ADHESIVE	Y	74
DCB2-36	11	22	121	19.1	62.6	Y	120	O	10	9	Y	FK44NC	N/A	82	ADHESIVE	Y	87
DCB2-37	11	22	121	19.1	62.6	Y	120	O	9	9	Y	FK44NC	N/A	83	ADHESIVE	Y	74

There are several likely factors for why there was a large difference in pristine bond strength. Environmental factors effect both the prepreg and the adhesive. Higher temperatures and high humidity are known to be very detrimental to the bonding process [58]. The data has been recorded for the humidity and temperature during the curing of the prepreg and the curing of the adhesive. Another factor that is not well understood is the material out-time for both the prepreg and the adhesive. Out-time is important for prepregs because the epoxy resin matrix is unstable at room temperatures [58].

One other factor is that there are several different fracture toughness values that could be calculated. There will be different fracture toughness values for the adherend,

the adhesive, and the interface, where the interfacial fracture toughness will vary based on the surface preparation method. The heavily contaminated samples had a near 100% adhesive failure mode as can be seen in Figure 35a. The failure mode can be determined by the color of each surface of the sample in the test area. The CFRP is black and the adhesive is pink. If there is the pink adhesive on one side and black CFRP on the other side, then the fracture propagated through the interface, separating the two, which is a cohesive failure. Adherend failure can be seen by having the black CFRP on both sides of the sample, and cohesive failure is seen when the pink adhesive is on both sides of the sample as can be seen in Figure 35b. The pristine bonds tended to have a mix of adherend and cohesive failure modes. This is another factor that could cause a wider range of fracture toughness values in the pristine samples. The failure mode could only be determined qualitatively by eye. Future work could implement image recognition software to quantify the failure mode percentage and then fracture toughness for each failure mode as used in the DARPA TRUST report [26].



(a)

(b)

Figure 35: Failure modes for (a) contaminated and (b) pristine DCB samples

## CONCLUSIONS

The CFRP adhesively bonded joint fabrication method developed in this thesis research allows for reliability in creating strong and very weak bonds. By using this method with consistent layup, curing process, sanding, and proper handling of the materials, reliable strong or very weak bonds can be fabricated. The use of water contact angle asks as a very strong indicator of the very weak or strong bond. The weak bonds are kissing bonds in that the dominant failure mode is adhesive failure, with a fracture toughness of less than 14% of the initiation fracture toughness of the strong bonds. The kissing bonds were also reliably fabricated when the contact angle was greater than 80 degrees. Strong bonds were produced reliably when the contact angle was less than 10 degrees. This behavior was consistent for both the out-of-autoclave material, Material 1, and the autoclave material, Material 2. The heavily contaminated lap joint samples had an average shear stress at failure of 32% of the average. The failure modes were also almost entirely adhesive for the lap joint samples.

This reliability in failure strength is useful for NDI tests. Because kissing bonds are difficult to create, according to industry professionals, creating kissing bonds repeatably will allow for NDI testing to be performed on a more consistent sample. Hopefully, this will lead to progress in detecting a kissing bond using any of the various NDI methods.

Although this thesis research developed a systematic method for creating and fabricating composite bonded joints with various degrees of bond strength, there are some limitations in the work. The largest limitation lies in the data analysis. This research

focused on the water contact angle as a simple and quick measure for determining strong and very weak bonds when combined with the rest of the fabrication methods. Much more data was taken throughout the fabrication and testing, such as the environmental data, out-time, cure pressure, cure cycle temperature, sanding grit, sanding tool, etc. This work did not make use of much of that important data or the other tools used, such as the FTIR and surface profiler. Also, minor changes in sanding due to human error could have had an effect on the failure mode for strong bonds. Because of the range of failure strength, particularly in the strong bonds, the contact angle also acts more like a guideline for a range of strength than a precise predictor of the strength.

There are several areas that future work could look into related to this thesis. Machine learning or some other analytical tool could be investigated to observe trends in the fabrication data and the bond strength. A more experimental approach could also be taken to examine the effects of the other factors. For example, the ambient temperature and humidity were not controllable during the testing. Varying these factors could result in a better understanding of the bond strength, particularly the strong sample's bond strength. One of the more interesting factors is the sanding. Although it may remove surface contaminants, it may also be damaging the fibers. An extensive look at the effect of sanding of various grits and perhaps material removed on the bond strength of pristine bonds would be insightful. Particularly if the failure mode were examined in relation to the sanding. A large amount of the pristine bonds failed with a mostly adherend failure mode. It is the author's suspicion that this could be in part due to the sanding damaging the fibers. As for the failure modes, a method for quantifying the failure modes would vastly improve the understanding of the failure. More analysis is necessary to determine

the usefulness for intermediate ranges of contact angles. Small investigations in the area seemed to result in a bond strength very close to the strong bonds. More data is required to see if there are trends, particularly with increased control of more variables in the process, such as environmental factors. This method also has room to expand and be improved through the use in-situ cure data. It is likely that combining the contact angle measurement with fabrication and environmental data will give allow for even more reliability to the adhesive bonding strength.

## References

1. J. Hale. "Boeing 787 from the Ground Up." *AERO - Boeing 787 from the Ground Up*, 2008, [www.boeing.com/commercial/aeromagazine/articles/qtr\\_4\\_06/article\\_04\\_2.html](http://www.boeing.com/commercial/aeromagazine/articles/qtr_4_06/article_04_2.html).
2. "A350 XWB Family." *Airbus*, [www.airbus.com/aircraft/passenger-aircraft/a350xwb-family.html](http://www.airbus.com/aircraft/passenger-aircraft/a350xwb-family.html).
3. *A Technology Roadmap for Joining and Repair of Advanced Polymer Matrix Composites*. Georgia Tech Manufacturing Institute, 2017, A Technology Roadmap for Joining and Repair of Advanced Polymer Matrix Composites.
4. G. Gardiner. "SAMPE Europe Highlights: Composites Face Challenges in next Commercial Airframes." *CompositesWorld*, CompositesWorld, 9 Apr. 2014, [www.compositesworld.com/blog/post/sampe-europe-highlights-composites-face-challenges-in-next-commercial-airframes](http://www.compositesworld.com/blog/post/sampe-europe-highlights-composites-face-challenges-in-next-commercial-airframes).
5. F. Fischer, et al. "Using Excimer Lasers to Clean CFRP Prior to Adhesive Bonding." *Reinforced Plastics*, vol. 57, no. 5, 2013, pp. 43–46., doi:10.1016/s0034-3617(13)70156-5.
6. H. Hocheng, and C.c. Tsao. "Effects of Special Drill Bits on Drilling-Induced Delamination of Composite Materials." *International Journal of Machine Tools and Manufacture*, vol. 46, no. 12-13, 2006, pp. 1403–1416., doi:10.1016/j.ijmachtools.2005.10.004.
7. F. Barthelat, et al 2003 Dynamic torsion testing of nanocrystalline coatings using high-speed photography and digital image correlation *Exp. Mech.* 43 331–40
8. D. Liu, et al. "A Review of Mechanical Drilling for Composite Laminates." *Composite Structures*, vol. 94, no. 4, 2012, pp. 1265–1279., doi:10.1016/j.compstruct.2011.11.024.
9. Federal Aviation Administration (September 8, 2009). Advisory Circular 20-107B, COMPOSITE AIRCRAFT STRUCTURE. [https://www.faa.gov/documentLibrary/media/Advisory\\_Circular/AC20-107B.pdf](https://www.faa.gov/documentLibrary/media/Advisory_Circular/AC20-107B.pdf)
10. B. Ehrhart, et al. "Non-Destructive Evaluation (NDE) of Aerospace Composites: Methods for Testing Adhesively Bonded Composites." *Non-Destructive Evaluation (NDE) of Polymer Matrix Composites*, 2013, doi:10.1533/9780857093554.2.220.
11. P. N. Marty, N. Desai, and J. Andersson, "NDT of kissing bond in aeronautical structures." 16th World Conference on NDT (WCNDT'04), Montreal, Canada, 2004.

12. C. Jeenjitkaew, and F.j. Guild. "The Analysis of Kissing Bonds in Adhesive Joints." *International Journal of Adhesion and Adhesives*, vol. 75, 2017, pp. 101–107., doi:10.1016/j.ijadhadh.2017.02.019.
13. S. Ebnesajjad, and C. Ebnesajjad. *Surface Treatment of Materials for Adhesive Bonding*. William Andrew, an Imprint of Elsevier, 2014.
14. S. I. Rokhlin, N. Wang, O. Lobkis, J.H. Cantrell, "Development of linear and nonlinear ultrasonic methodology for quantitative assessment of environmental degradation of adhesive bonds." Ohio State University and NASA Langley RC, 2010.
15. B. K. Siu, "System and method for laser ultrasonic bond integrity evaluation." U.S. Patent 6,490,047, issued December 3, 2002.
16. S. Hirsekorn, A. Koka, A. Wegner, and W. Arnold, "Quality assessment of bond interfaces by nonlinear ultrasonic transmission." AIP Conference Proceedings, 509(1), 1367-1374, 2000.
17. S. Hirsekorn, "Nonlinear transfer of ultrasound by adhesive joints—a theoretical description." *Ultrasonics* 39(1): 57-68, 2001.
18. R. A. Smith, V.L. Weise, and R.P. Dalton, "The potential for advanced ultrasonic detection of weak adhesion." QinetiQ Ltd: 1-5, 2003.
19. M. G. Zaitsev, "Influence of "weak" bonds in macromolecules on the activation energies of fracture of oriented polymers." *Polymer Science U.S.S.R.*, 28(2): 435-442, 1986.
20. R. B. Heslehurst, "Optical NDT of adhesively bonded joints." *Materials Evaluation*, 67(7): 837-842, 2009.
21. R. H. Bossi, K. Housen, and W. Shepherd, "Application of stress waves to bond inspection." SAMPE Proceedings, Long Beach, CA, 2004.
22. R. H. Bossi, K. Housen, C. Walters, and Boeing Phantom Works, "Laser bond inspection device for composites: Has the holy grail been found." *NTIAC Newsletter* 30(2), 2005.
23. M. Arrigoni, S. E. Kruger, A. Blouin, D. Lévesque, B. Arsenault, J. P. Monchalain, M. Boustie, and L. Berthe, "Adhesive bond testing by laser induced shock waves."
24. C. Wang, and C. Duong. "Design of Scarf and Doubler-Scarf Joints." *Bonded Joints and Repairs to Composite Airframe Structures*, 2016, pp. 83–112., doi:10.1016/b978-0-12-417153-4.00004-9.
25. L. Sorrentino, et al. "Surface Treatment of CFRP: Influence on Single Lap Joint Performances." *International Journal of Adhesion and Adhesives*, vol. 85, 2018, pp. 225–233., doi:10.1016/j.ijadhadh.2018.06.008.

26. G. Gardiner. "Building TRUST in Bonded Primary Structures." *CompositesWorld*, CompositesWorld, 1 Apr. 2015, [www.compositesworld.com/articles/building-trust-in-bonded-primary-structures](http://www.compositesworld.com/articles/building-trust-in-bonded-primary-structures).
27. M. H. Ata, et al. "Failure Mode and Failure Load of Adhesively Bonded Composite Joints Made by Glass Fiber-Reinforced Polymer." *Journal of Failure Analysis and Prevention*, vol. 19, no. 4, Jan. 2019, pp. 950–957., doi:10.1007/s11668-019-00678-y.
28. B. Z. Jang. "Control of Interfacial Adhesion in Continuous Carbon and Kevlar Fiber Reinforced Polymer Composites." *Composites Science and Technology*, vol. 44, no. 4, 1992, pp. 333–349., doi:10.1016/0266-3538(92)90070-j.
29. C. Jeenjitkaew, et al. "Morphology and Surface Chemistry of Kissing Bonds in Adhesive Joints Produced by Surface Contamination." *International Journal of Adhesion and Adhesives*, vol. 30, no. 7, 2010, pp. 643–653., doi:10.1016/j.ijadhadh.2010.06.005.
30. H.W. Schreier 2003 Investigation of two and three-dimensional image correlation techniques with applications in experimental mechanics PhD Thesis University of South Carolina
31. M. Sjodahl and L. R. Benckert 1993 Electronic speckle photography: analysis of an algorithm giving the displacement with subpixel accuracy *Appl. Opt.* 32 2278–84
32. M. Sjodahl and L.R. Benckert 1994 Systematic and random errors in electronics speckle photography *Appl. Opt.* 33 7461–71
33. B. K. Bay 1995 Texture correlation—a method for the measurement of detailed strain distributions within trabecular bone *J. Orthop. Res* 13 258–67
34. D. Zhang, X. Zhang and G. Cheng 1999 Compression strain measurement by digital speckle correction *Exp. Mech.* 39 62–5
35. P. Zhou and K. E. Goodson 2001 Subpixel displacement and deformation gradient measurement using digital image/speckle correlation *Opt. Eng.* 40 1613–20
36. D. J. Chen, F. P. Chiang, Y. S. Tan and H. S. Don 1993 Digital speckle-displacement measurement using a complex spectrum method *Appl. Opt.* 32 1839–49
37. G. R. Gaudette, J. Todaro, I. B. Krukenkamp and F. P. Chiang 2001 Computer aided speckle interferometry: a technique for measuring deformation of the surface of the heart *Ann. Biomed. Eng.* 29 775–80
38. T. S. Smith, B. K. Bay and M. Rashid 2002 Digital volume correlation including rotational degrees of freedom during minimization *Exp. Mech* 42 272–8

39. B. Pan, et al. "Two-Dimensional Digital Image Correlation for in-Plane Displacement and Strain Measurement: a Review." *Measurement Science and Technology*, vol. 20, no. 6, 2009, p. 062001., doi:10.1088/0957-0233/20/6/062001.
40. N. Sabate, et al 2006 Measurement of residual stresses in micromachined structures in a microregion *Appl. Phys. Lett.* 88 071910
41. J. Keller, et al 2006 FibDAC—residual stress determination by combination of focused ion beam technique and digital image correlation *Mater. Sci. Forum* 524–525 121–6
42. J. Kang, et al 2005 Microscopic strain mapping using scanning electron microscopy topography image correlation at large strain *J. Strain Anal. Eng. Des.* 40 559–70
43. M. Kawahashi and H. Hirahara 2000 Velocity and density field measurements by digital speckle method *Opt. Laser Technol.* 32 575–82
44. Kulkarni, S. Vitthal and S. Charles. "Membrane Materials." *Membrane Contactors: Fundamentals, Applications and Potentialities Membrane Science and Technology*, 2006, pp. 40–104., doi:10.1016/s0927-5193(05)80003-8.
45. J. Comyn, "Contact Angles and Adhesive Bonding." *International Journal of Adhesion and Adhesives*, vol. 12, no. 3, 1992, pp. 145–149., doi:10.1016/0143-7496(92)90045-w.
46. A. Rein and P.L. Tang, "Analysis of Plasma Treated Carbon Fiber Reinforced Polymer (CFRP) Composites by Portable Fourier Transform Infrared Spectroscopy (FTIR)." Agilent Technologies, I., 2015.
47. J. M. Chalmers, "INFRARED SPECTROSCOPY | Sample Presentation." *Reference Module in Chemistry, Molecular Sciences and Chemical Engineering*, 2013, doi:10.1016/b978-0-12-409547-2.00254-7.
48. V. Tucureanu, A. Matei, and A.M. Avram, "Ftir Spectroscopy for Carbon Family Study," *Crit Rev Anal Chem*, 46(6), 502-20, 2016.
49. N.K. Afseth, and A. Kohler, 2012, "Extended Multiplicative Signal Correction in Vibrational Spectroscopy, a Tutorial," *Chemometrics and Intelligent Laboratory Systems*, 117, 92-99.
50. P. Bassan, 2011, "Light Scattering During Infrared Spectroscopic Measurements of Biomedical Samples," (Ph.D.), University of Manchester.
51. *Organic Chemistry with a Biological Emphasis* by Tim Soderberg (the University of Minnesota, M. Vibrations and Rotations of Molecules: Infrared and Microwave Spectroscopy. Journal of colloid and interface science Feb 2, 2016; Available from: [https://chem.libretexts.org/Courses/University\\_of\\_California\\_Davis/UCD\\_Chem\\_002 CH/U](https://chem.libretexts.org/Courses/University_of_California_Davis/UCD_Chem_002_CH/U)

- NIT\_IV%3A\_MOLECULAR\_SPECTROSCOPY/20.2%3A\_Vibrations\_and\_Rotations\_of\_Molecules%3A\_Infrared\_and\_Microwave\_Spectroscopy.
52. ASTM International. D5868-01(2014) *Standard Test Method for Lap Shear Adhesion for Fiber Reinforced Plastic (FRP) Bonding*. West Conshohocken, PA, 2014. Web. 20 Nov 2019. <https://doi.org/10.1520/D5868-01R14>
  53. ASTM International. *D5528-13 Standard Test Method for Mode I Interlaminar Fracture Toughness of Unidirectional Fiber-Reinforced Polymer Matrix Composites*. West Conshohocken, PA, 2013. Web. 20 Nov 2019. <https://doi.org/10.1520/D5528-13>
  54. M. Davis and J. Tomblin, “Best Practice in Adhesive-Bonded Structures and Repairs”, Department of Transportation FAA. Report No: DOT/FAA/AR-TN06/57.
  55. B. Boesl, “Effect of Surface Contamination on Composite Bond Integrity and Durability.” Nov. 2019.
  56. C. Jeenjitkaew, et al. “Morphology and Surface Chemistry of Kissing Bonds in Adhesive Joints Produced by Surface Contamination.” *International Journal of Adhesion and Adhesives*, vol. 30, no. 7, 2010, pp. 643–653., doi:10.1016/j.ijadhadh.2010.06.005.
  57. I. U. Ojalvo, and H. L. Eidinoff. “Bond Thickness Effects upon Stresses in Single-Lap Adhesive Joints.” *AIAA Journal*, vol. 16, no. 3, 1978, pp. 204–211., doi:10.2514/3.60878.
  58. I. A. Ashcroft, et al. “Adhesive Bonding of Fibre Reinforced Polymer Composite Materials.” *Assembly Automation*, vol. 20, no. 2, 2000, pp. 150–161., doi:10.1108/01445150010321797.
  59. P. W. R. Beaumont, “Structural Integrity and the Implementation of Engineering Composite Materials.” *Structural Integrity and Durability of Advanced Composites*, 2015, pp. 353–397., doi:10.1016/b978-0-08-100137-0.00015-8.